nature reviews bioengineering

https://doi.org/10.1038/s44222-023-00025-9

Review article

Check for updates

Smart micro- and nanorobots for water purification

Mario Urso [1,2], Martina Ussia [1,2] & Martin Pumera [1]

Abstract

Less than 1% of Earth's freshwater reserves is accessible. Industrialization, population growth and climate change are further exacerbating clean water shortage. Current water-remediation treatments fail to remove most pollutants completely or release toxic by-products into the environment. The use of self-propelled programmable micro- and nanoscale synthetic robots is a promising alternative way to improve water monitoring and remediation by overcoming diffusion-limited reactions and promoting interactions with target pollutants, including nano- and microplastics, persistent organic pollutants, heavy metals, oils and pathogenic microorganisms. This Review introduces the evolution of passive micro- and nanomaterials through active micro- and nanomotors and into advanced intelligent micro- and nanorobots in terms of motion ability, multifunctionality, adaptive response, swarming and mutual communication. After describing removal and degradation strategies, we present the most relevant improvements in water treatment, highlighting the design aspects necessary to improve remediation efficiency for specific contaminants. Finally, open challenges and future directions are discussed for the real-world application of smart micro- and nanorobots.

Sections

[1]Central European Institute of Technology, Brno University of Technology, Brno, Czech Republic. [2]These authors contributed equally: Mario Urso, Martina Ussia. e-mail: martin.pumera@ceitec.vutbr.cz

Introduction

Water is vital for all forms of life. However, of the Earth's freshwater, less than 1% is estimated to be accessible, and its contamination represents one of the most severe ecological threats[1,2]. Furthermore, clean water shortage is intensifying owing to the increasing global demand associated with population growth, industrialization and climate change[3]. Contaminants such as plastic waste, heavy metals, persistent organic pollutants (including pharmaceuticals and pesticides) and oil spills are associated with substantial ecological risks. Once within the aquatic ecosystem, contaminants can cause irreversible accumulative, recurrent, carcinogenic, mutagenic and other detrimental effects on the aquatic flora and fauna, while their propagation through the food chain further amplifies the associated risks[4]. Moreover, aqueous protozoan, bacterial and viral pathogens can cause the spread of typhoid, cholera, salmonella and other diseases. In addition, higher global temperatures increase the concentration of nutrients such as carbon, nitrogen and phosphate in raw water, which favours the regrowth of opportunistic pathogens mainly caused by antimicrobial-resistant pathogens[1,2]. In this context, bacterial biofilm formation onto industrial pipes and water lines results in a slower water flow and corrosion of the tubes, thus reducing the hydraulic efficiency of power plants and further compromising the safety of drinking-water distribution systems[5–7]. Although these biological risks might seem more relevant for developing regions, industrialized regions will also need to adapt to the scarcity of clean water resources, requiring innovative solutions for frequent (re)use of grey water (such as from washing machines and dishwashers) and natural water bodies to ensure drinking water supplies.

The concept of 'water remediation' dates back to Sanskrit, ancient Greek and Egyptian writings around 2000 BC, from Hippocrates with the discovery of water's healing properties, the Roman aqueducts and Archimedes' screw, up to modern-era treatments, including filtration systems with coagulation and sedimentation. Furthermore, water chlorination and desalination methods, as well as the use of advanced oxidation processes and nanotechnologies, have reduced the hazards and illnesses related to contaminated drinking-water distribution systems[3]. Despite these advances, 75% of water bodies remain at ecological risk[1]. During water remediation, most pollutants are not completely removed from contaminated areas or are merely degraded, releasing toxic by-products into the environment.

Owing to their active motion, self-propelled programmable micro- and nanoscale synthetic robots provide exciting opportunities to improve water monitoring and remediation processes, enhancing treatment efficiency by overcoming diffusion-limited reactions and promoting interactions with target pollutants[8–15]. In this Review, we describe the path to engineering small-scale materials into intelligent micro- and nanorobotic machines that can autonomously move to accomplish predetermined tasks. In particular, we focus on micro- and nanorobots that remove and degrade water contaminants, ranging from nano- and microplastics to organic molecules, heavy metals, oil spills and microorganisms. Finally, we discuss practical challenges and future research directions, proposing systems suitable for real-world applications.

From materials to robots

Robots are machines programmed to perform specific tasks autonomously or under human supervision. Small-scale robots (<100 µm), initially referred to as 'micro- and nanomotors', are micro- and nanostructured materials capable of harvesting energy from the surrounding environment and converting it into locomotion[16,17]. These tiny devices benefit from the synergy between their motion attributes and their unique size-, shape- and structure-dependent physicochemical properties at the micro- and nanoscale. Furthermore, they show superior performance compared to passive matter (for example, conventional static micro- and nanomaterials) in all areas, including water remediation[18–25]. The active motion of micro- and nanomotors drives the movement of the surrounding fluid, improving the mass transfer of chemical reactions, which are limited to passive diffusion in static approaches. This process facilitates the interaction between the motors and the water contaminants, resulting in shorter purification times. As the complexity of the required functions increased, for example, catching selected pollutants or moving the robots in groups to improve removal and degradation efficiency, the design of micro- and nanomotors became more sophisticated[10,26]. The introduction of propulsion, multifunctionality, adaptation to the environment, collective behaviours and mutual communication have transformed micro- and nanomaterials into intelligent micro- and nanorobots (Fig. 1). To realize self-propulsion, reliable fabrication methods are needed to induce asymmetry in the material's structure, allowing it to break the symmetry of a local field and 'swim'[27–30] (Table 1). Therefore, depending on the motion mechanism, micro- and nanorobots can be classified as fuel-driven or externally driven[31] (Fig. 2).

Fuel-driven micro- and nanorobots

Fuel-driven micro- and nanorobots, also known as 'chemical' or 'catalytic', exploit the reaction between a catalyst and a chemical fuel (or substrate) to move[32–35]. Despite its toxicity, hydrogen peroxide (H_2O_2) is

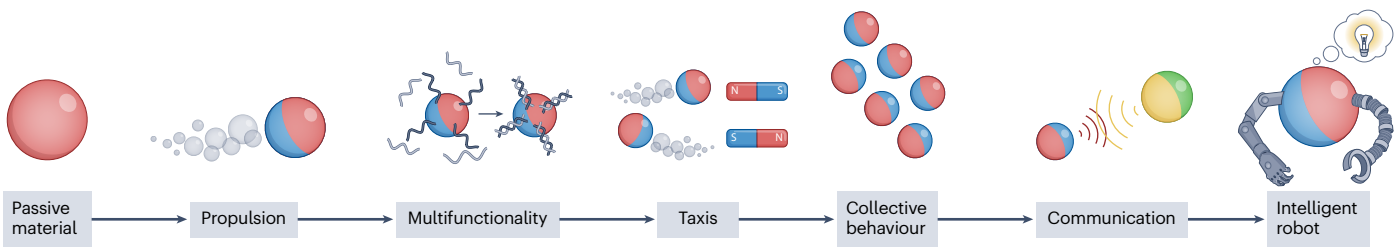

Fig. 1 | From passive materials to intelligent robots. Micro- and nanorobots are designed using micro- and nanomaterials and introducing: propulsion, the ability to move spontaneously by consuming a chemical fuel or under exposure to an external field; multifunctionality, the ability to perform multiple specific tasks; taxis, the adaptive response to environmental stimuli such as gradients of chemical species (chemotaxis), light (phototaxis) or magnetic fields (magnetotaxis); collective behaviour, the cooperative action of robot ensembles to improve the efficacy of a process or to perform complicated tasks beyond an individual's capability; communication, through which neighbouring robots can operate in a coordinated and synchronized manner and exchange information. The scheme illustrates an example of a bubble-propelled Janus robot in which the red and blue hemispheres represent the structural–functional and engine sides, respectively. The sizes of microrobots and nanorobots are 1–100 µm and <1 µm, respectively.

Table 1 | Main micro- and nanorobot fabrication methods

Fabrication method	Technique	Structure	Advantages	Limitations
Electrochemical	Membrane template-assisted electrochemical deposition	Micro- and nanotubes, microrods, nanowires	Low-cost, organic and inorganic material preparation	Large-scale production and robot geometries limited by membrane features (pore size, shape)
Chemical	Polymerization, hydrothermal reaction, precipitation, solvent extraction and evaporation, functionalization	Symmetric and asymmetric micro-and nanoparticles	Simple equipment, low-cost and large-scale production	Reproducibility
Physical	Physical vapour deposition (sputtering, evaporation, atomic layer deposition), direct laser writing	Anisotropic structures, coatings for Janus structures	High control and reproducibility	Expensive equipment
Bio-based	Bio-templated robot fabrication, bio-hybrids (microorganisms modified with micro- and nanoparticles)	Organic and inorganic micro- and nanostructures, self-motile structures for hybrid robots	Low-cost, sustainability, and abundance of bio-templates	Short robot lifespan
Self-assembly	Layer-by-layer assembly, macromolecular assembly, shape transformation	Vesicles, Janus capsules, polymersomes	Simple equipment, low-cost, sustainability, versatility, bio-inspired and biodegradable materials preparation	Mostly fuel-driven
3D printing	Fused deposition modelling, selective laser sintering, direct ink writing	3D and 4D structures	Low-cost and large-scale production, high control and reproducibility	Limited resolution and range of suitable materials

the most frequently used fuel and the expensive noble metal platinum (Pt) is its most efficient decomposition catalyst, resulting in micro- and nanorobotic propulsion by bubble ejection or self-phoresis[36]. The latter is the spontaneous motion of a particle in response to the generation of a quantity gradient, such as solute concentration (self-diffusiophoresis), electric potential (self-electrophoresis) or temperature (self-thermophoresis). For example, Pt microrockets self-propel in H_2O_2 owing to the continuous jet stream of O_2 bubbles (Fig. 2a), which also produce powerful thrusts and motility in high-ionic-strength media, such as seawater[37,38]. Enzymes, such as catalase, urease and glucose oxidase, are the biological counterpart of inorganic catalysts[39–41]. Micro- and nanorobots with uneven distribution of catalase (an enzyme catalysing the decomposition of H_2O_2) undergo bubble propulsion in H_2O_2, whereas urease and glucose oxidase hydrolyse more biocompatible substrates, like urea and glucose, generating a product gradient for micro- and nanorobotic self-phoresis (Fig. 2b). However, their use is restricted to biomedical applications where the substrates are naturally present, for example, the bladder for urea[42]. Disintegration of the robots is mediated by catalytic reactions that simultaneously consume the robot's engine and fuel, similar to the reaction between Mg and water[43–45] (Fig. 2c). However, fuel-driven micro- and nanorobots suffer from poor control over the motion (on–off, directionality) and limited life span.

Externally driven micro- and nanorobots

Externally driven micro- and nanorobots overcome the limitations of fuel-driven ones by gathering energy from external fields, including light, acoustic and electromagnetic fields. Of these sources, sunlight is particularly beneficial, being a natural, abundant and renewable form of energy that can trigger several degradation mechanisms at the same time[46–49]. The motion of light-powered robots originates from the generation of electron–hole pairs (e^-–h^+) in an irradiated photoactive material. For example, by illuminating a semiconductor material with photon energies larger than its bandgap, electrons are promoted to the conduction band, leaving holes in the valence band. These photogenerated carriers catalyse photochemical reactions that result in motion by bubble propulsion or self-phoresis. A metal–semiconductor junction is often required to prevent photogenerated carriers recombining within the semiconductor or to break the semiconducting material's symmetry[50,51]. The motion mechanism of a typical metal–semiconductor Janus micro- or nanorobot comprises photogenerated carriers that lead to the oxidation and reduction of water at the two sides of the robot (Fig. 2d). Specifically, the semiconductor side acts as a source of protons (H^+), which are consumed at the metal side (the proton sink), establishing a gradient of charges, and consequently, a local electric field driving the micro- or nanorobot's movement by self-electrophoresis. However, single-component metal-coating-free micro- and nanorobots can also move under light owing to their inherent asymmetry or asymmetric illumination[52]. The main limitation of light-powered robots is the decreasing light intensity with depth and the inefficient self-electrophoresis in high-ionic-strength media (seawater). By contrast, magnetic fields can operate micro- and nanorobots in any medium with great manoeuvrability[53,54]. Rather than mere magnetic-mediated attraction–repulsion, these robots move by magnetophoresis in magnetic-field gradients or by torque transfer under rotating magnetic fields. For example, helical propellers in a rotating magnetic field convert their rotation into a translational movement[55] (Fig. 2e). Unlike light-driven robots, magnetically driven robots are not autonomous and are limited by the high cost and size constraints associated with the magnetic setup[56]. Electric field propulsion, achieved by combining materials with different polarizability, is similar to magnetic propulsion, including fuel-free controllable motion[57]. Acoustic fields can also actuate different micro- and nanorobot designs, such as bimetallic microrods or asymmetric nanowires, owing to the pressure exerted by acoustic radiation[58–61] (Fig. 2f). Ultrasound fields are harmless to the human body, which is why they have been principally used for biomedical applications, allowing rapid cell internalization, intracellular propulsion and delivery of therapeutic agents[62,63].

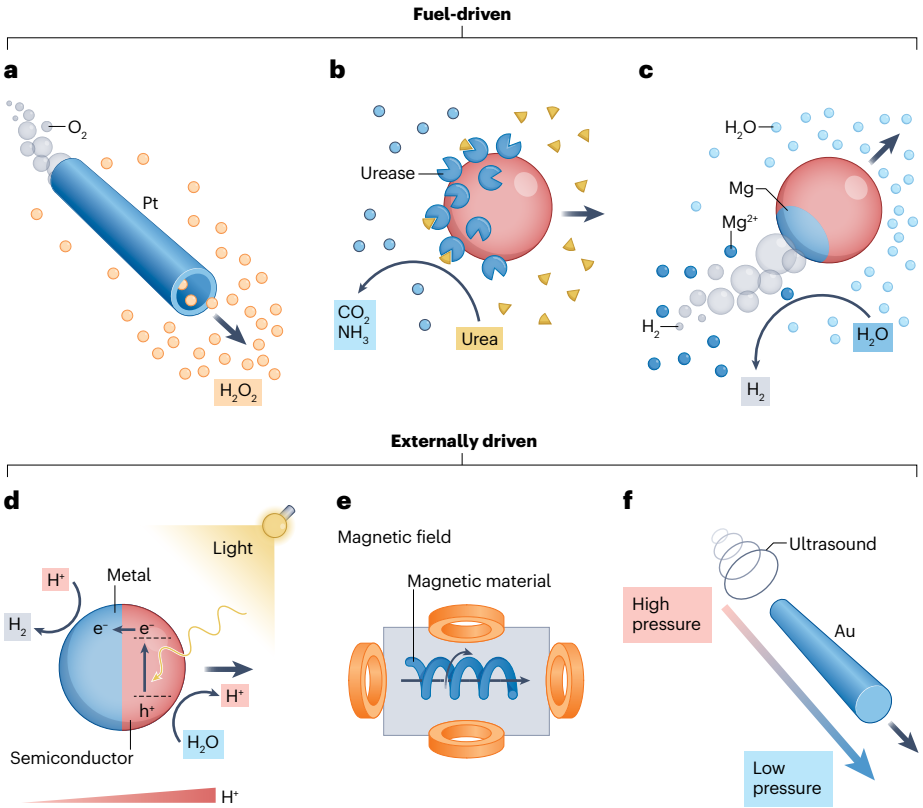

Fig. 2 | Motion mechanisms of fuel-driven and externally driven micro- and nanorobots. a, Pt microrockets self-propel owing to the catalysed decomposition of H_2O_2 into O_2 bubbles, whose expulsion results in a powerful thrust. **b**, Enzyme-powered nanorobots are based on the uneven immobilization of an enzyme (such as urease), catalysing the hydrolysation of a substrate (urea), resulting in a product gradient that drives their motion by self-phoresis. **c**, The engine of disintegrating robots decomposes during propulsion, such as for Mg-based microrobots, whose reaction in water produces a stream of H_2 bubbles at the expense of the Mg core. **d**, Metal–semiconductor Janus micro- and nanorobots move under light irradiation owing to the photogenerated electron–hole (e^-–h^+) pairs within the semiconductor. Oxidation and reduction of water occur at both sides of the robot, establishing a gradient of protons (H^+) and the resulting local electric field, which induces motion by self-electrophoresis. **e**, Upon exposure to a rotating magnetic field, magnetic helical robots translate the rotational motion generated by orthogonal coil pairs into a translational motion that can be wirelessly navigated with high precision. **f**, Micro- and nanorobots can move upon pressure exerted by acoustic fields. Red and blue structures represent the structural–functional component and the engine of the robot, respectively.

Multifunctional micro- and nanorobots

In addition to simple swimming, robots are also required to perform tailored tasks in specific applications. Multifunctionality is imparted to micro- and nanorobots by integrating different modules, such as organic or inorganic molecules and materials[64–67]. Each micro- and nanorobot's module has a defined role: the structural material provides a robust scaffold, the engine is responsible for the motion, the imaging material enables traceability, the magnetic material introduces magnetic properties (such as collectability under magnetic fields) and the surface material interacts with the environment, including water contaminants in the robot's proximity through intrinsic properties or surface functional groups (ranging from simple molecules to supramolecular structures and polymers). For example, DNA-engineered micro- and nanorobots exploit the self-propulsion, programmability and specificity of Watson–Crick base pairing for the intracellular detection of cancer biomarkers or gene delivery[68]. However, the choice of single-task or multi-purpose robots must be thoroughly assessed, because integrating multiple units entails several fabrication, assembly and scaling challenges[69].

Although small-scale robots have shown promising results in laboratory settings, real-world scenarios are complex and dynamic. Propulsion and movement can easily be influenced by variations in the chemical composition of the swimming media or from exposure to unexpected stimuli. Therefore, similar to living organisms, smart robots need to exhibit adaptive responses to dynamically changing environments. For example, the *Escherichia coli* bacterium uses receptors to sense the concentration of chemicals (such as nutrients) in its surroundings and move towards richer spots[70]. Another example is the diel vertical migration of plankton in aquatic ecosystems; these organisms move to the surface at night to access food and avoid predators and return to the bottom region during the day[71]. Taxis (mainly chemotaxis, phototaxis and magnetotaxis) in micro- and nanorobots relies on stimulus-mediated mechanisms[72,73]. For example, chemotactic robots move according to concentration gradients of chemicals, such as their fuel[74–76]. As they move along the gradient, their diffusivity increases owing to the enhanced catalytic reaction rate at higher fuel concentrations (Fig. 3a). Phototactic micro- and nanorobots sense the direction of light, orient and move towards (positive phototaxis) or away

from it (negative phototaxis)[77–79] (Fig. 3b). Phototaxis has generally been observed in highly asymmetric structures. The most renowned example of an artificial phototactic microswimmer consists of a Janus nanotree formed by a silicon trunk and titanium dioxide (TiO_2) branches with chemically programmable negative or positive phototaxis, mimicking the behaviour of natural green algae[80]. Gravitaxis, the movement in response to gravity, is another form of behavioural response. This phenomenon is observed in micro- and nanorobots with asymmetric mass distribution or structure, in which they move in the opposite direction of gravity. For example, some light-driven micro- and nanorobots show a form of gravitaxis in response to light (like the diel vertical migration), typically referred to as 'negative photogravitaxis'[81–83] (Fig. 3c). Magnetotactic micro- and nanorobots adjust their motion according to the direction of magnetic field gradients or dynamic magnetic fields to minimize energy consumption[84–86]. For example, they can be attracted or repelled by a magnetic field upon polarity inversion (Fig. 3d).

Collective micro- and nanorobots

Collective animal behaviour involves the execution of tasks beyond the single animal's capability. For example, ant colonies self-assemble into robust 'bridges' to march across gaps in terrains, whereas starlings' synchronized motion as shape-shifting clouds allows them to frighten predators. These behaviours have inspired artificial swarming micro- and nanorobots[87]. Compared to single robots, micro- and nanorobot swarms provide superior efficiency, robustness and flexibility. For example, a group of robots can perform a desired task faster than a single robot can and accomplish size-dependent operations, such as the transport of large cargoes, which requires the cooperation of several robots. The group perceives broader environmental variations compared to single robots, and, in the event of a robot's failure, it can still complete the assigned task[88]. The fundamental feature of micro- and nanorobot swarms is the collective motion of its constituents. Typically, tactic micro- and nanorobots manifest coordinated movements in response to energy gradients[89]. However, practical applications require swarms to adapt to environmental changes through self-organization and reconfigurability in shape and function. All these behaviours rely on physico-chemical interactions between the robots[90–93]. For example, light-powered magnetic microrobots spontaneously assemble into self-motile 'snake-like' microchains owing to the particles' shape-modulated magnetic dipole–dipole interactions[94]. Furthermore, using external magnetic fields, microrobots can reversibly switch from a dispersed to an aggregate state, allowing them to explore their surroundings, move as a group to overcome obstacles and rotate or transport microscale objects[95]. Integrating the functions of contaminant removal and degradation into robotic swarms can thus be a promising approach.

Communication between micro- and nanorobots or with the environment is another essential feature to ensure synchronized maneuvering of swarms, which still remains one of the main challenges in micro- and nanorobotics. For example, robots exchange chemical signals, such as the release of small molecules or ions, producing a chemical gradient to attract, repel, accelerate or decelerate other robots[96]. Moreover, long-range hydrodynamic communication between micro- and nanorobots produces a 'hit and run' response whereby a robot acts as a 'leader', collecting smaller particles ('followers') and fighting

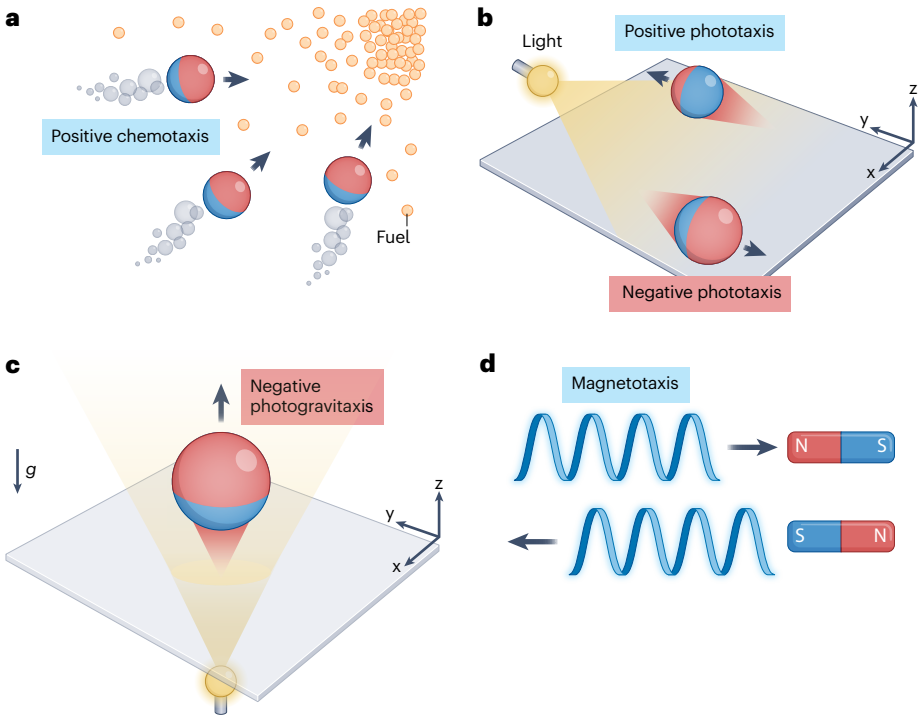

Fig. 3 | Tactic micro- and nanorobots. a, Positive chemotaxis of bubble-propelled Janus micro- and nanorobots moving towards the region with a higher fuel concentration. **b**, Light-driven Janus micro- and nanorobots move towards (positive phototaxis) or away from (negative phototaxis) the light source on a plane. **c**, A light-driven Janus robot irradiated from beneath moves upwards (opposite to gravity (*g*)), leading to negative photogravitaxis. **d**, Magnetotaxis of a magnetic helical robot moving towards or away from a magnetic field upon inverting its polarity. Red and blue structures represent the structural–functional component and the engine of the robot, respectively.

to gather the followers of a competitor[97]. This intriguing response could be used to design micro- and nanorobots capable of recognizing more persistent and toxic pollutants in water and communicating this information to other robots in the swarm, gathering them around the targeted contaminant to ensure its removal or degradation. However, exchanging such complex information and functions between robots in real-world settings is still far from being accessible.

Robots for water remediation

Micro- and nanorobots aim to accelerate and improve the water decontamination process. The synergistic action between their active motion and their material properties enhances the adsorption of soluble organic pollutants and heavy metals at the solid–liquid interface (Table 2). Specifically, once the target contaminants approach the robots' surface, a stable network of weak interactions is established through a physisorption mechanism, primarily electrostatic, without any external agitation. Electrostatic interactions refer to the positive or negative surface charge that molecules or particles acquire when immersed in a liquid medium and are strongly influenced by its pH and ionic strength[98]. Micro- and nanorobots can be programmed to possess a surface charge opposite to that of the target contaminants by functionalizing them with specific molecules or polymers or by modifying the solution parameters[99] (Fig. 4a). Impurities also possess a surface charge, allowing their capture, transport and release by electrostatic forces. For example, plastic-based debris is composed of polymers with negatively or positively charged functional end-groups. By properly modifying the micro- or nanorobot's surface charge through adjustments to the solution pH, it is possible to promote a reversible 'on the fly' adsorption or desorption of contaminants.

Establishing a stable and robust contact between the active robot and the passive contaminant is crucial for the removal process, but pH-dependent electrostatic forces might lack sufficient strength. To improve adherence, polydopamine (PDA) has been used as a sticky coating on robots to mimic the adhesive properties of marine mussels[100] (Fig. 4b). PDA has a structure similar to 3,4-dihydroxy-L-phenylalanine (DOPA), a natural polyaminoacid secreted by mussels that allows them to firmly adhere to solid surfaces and resist sea waves[10]. An alternative approach to facilitate contact with contaminants exploits strong and attractive phoretic interactions (Fig. 4c), which induce collective behaviours, assemblies or migration of passive particles owing to the generated (or modified) local gradients around the robots in response to diffusiophoretic, electrophoretic or thermophoretic mechanisms[100,101]. However, these strategies fail to permanently remove the adsorbed contaminants and further disposal is required. To overcome this issue, an ecofriendly approach that avoids the generation of secondary pollutants is to use advanced oxidation processes; these were introduced in 1987 as a class of water-treatment methods involving the production of highly reactive chemical species in "sufficient quantity to affect water purification"[102,103], including O_2, O_3 or H_2O_2 as oxidants, light irradiation and catalysts. The process consists of producing strong oxidizing agents called 'reactive oxygen species' (ROS), such as $OH^{\bullet}$, $O_2^{\bullet-}$, $O_2^{2\bullet}$ and $^1O_2$, through chemical or photochemical reactions. These ROS react with water contaminants, which are then cleaved into smaller compounds until their complete mineralization into CO_2 and water.

Fenton, Fenton-like, photo-Fenton reactions and heterogeneous photocatalysis are the most recurrent advanced oxidation processes used in water remediation by micro- and nanorobots. Fenton reactions are activated by Fe^{2+} or Fe^{3+} in H_2O_2, resulting in the production of $OH^{\bullet}$. Robots composed of Fe-based materials undergo corrosion in H_2O_2, catalysing the Fenton reaction (Fig. 4d). Similarly, a Fenton-like reaction refers to the same process induced by other catalysts, such as metals at lower oxidation states (for example, Pt). By contrast, heterogeneous photocatalysis is based on irradiating a photocatalytic material (semiconductor or photosensitizer) with photons having energy equal to or greater than its bandgap, generating electron-hole (e^-–h^+) pairs that migrate to the photocatalyst's surface and produce ROS upon reaction with water and O_2 (Fig. 4e). Micro- and nanorobots made of photocatalytic iron oxides, such as α-Fe_2O_3 (haematite), can also catalyse the photo-Fenton process in H_2O_2 by generating ROS through the reaction of photogenerated electrons with H_2O_2 (Fig. 4e). It is worth noting that light-powered micro- and nanorobots are particularly advantageous for water remediation because they use light both to move and simultaneously to degrade pollutants by photocatalysis or the photo-Fenton reaction. However, considering that adsorption is necessary to initiate the photocatalytic process, it is often challenging to distinguish the effective contribution of the motion-enhanced adsorption from the degradation. A low-cost and sustainable alternative to advanced oxidation processes is to use enzyme-mediated bioremediation. This method relies on natural enzymes, such as those secreted by microorganisms, to lower the activation energy required 'to digest' pollutants[104]. Moreover, enzymes can also be immobilized on synthetic micro- and nanorobots to use this mechanism (Fig. 4f).

Water decontamination from pathogenic microorganisms using micro- and nanorobots also benefits from complementary approaches. While moving, robots can rapidly release bactericidal agents (for example, silver ions (Ag^+)) in a controllable manner, resulting in bacteria elimination[105–107] (Fig. 4g). Self-propelled micro- and nanorobots can also erode bacterial biofilms from surfaces through a 'brush-like' effect[108] (Fig. 4h). In this case, the bacteria are only physically removed from the surface, therefore an additional step is required for their elimination. For example, selected antibacterial agents (such as antibiotics) can be chemically linked or physically adsorbed on the robots' surface. The carried antibiotic is then released on the residual bacteria to trigger a 'kill-n-clean' method that destroys all debris while avoiding recolonization[109] (Fig. 4i).

Nano- and microplastics

Plastics are synthetic materials made of polymer chains, that is, monomers linked by covalent bonds. Owing to their high adaptability, durability, flexibility, low weight and cost, plastics manufacturing has increased exponentially since the 1950s, making them ubiquitous in our lives. However, plastics are difficult to eliminate and they mainly accumulate in marine environments[110], where they fragment into smaller and more hazardous particles, namely, microplastics (<5 mm) and nanoplastics (<1 μm)[111]. Polyethylene, polypropylene and polystyrene are among the most recurrent ones. Their physicochemical properties mean that nano- and microplastics adsorb pollutants on their surfaces and support the growth of bacterial biofilms. They can propagate through the food chain or directly contaminate drinking-water distribution systems, posing a danger to the health of all living beings. Microplastics have already been detected in human blood, highlighting the importance of developing effective and definitive strategies for their elimination[112].

The first attempts at using micro- and nanorobots for microplastic sequestration exploited the active movement of light-driven Au–Ni–TiO_2 microrobots as self-propelled micromachines[101]. These microrobots propel themselves under ultraviolet (UV) light irradiation in water and H_2O_2 by self-electrophoresis, capturing microplastics

Table 2 | Summary of selected micro- and nanorobots for water remediation

Robot	Fabrication method	Size	Motion mechanism	Pollutant	Adsorption and degradation mechanism	Efficiency	Ref.
Nano- and microplastics							
Au–Ni–TiO_2	Chemical	700 nm	UV light	Microplastics (personal-care products in the Baltic sea)	Phoretic interactions and shovelling	67% in 40 s	101
Ni–SPGs	Biotemplated	~30 μm	Magnetic	Polystyrene beads	Non-contact shovelling	~75%	113
Fe_2O_3–MnO_2	Hydrothermal and annealing	~5 μm	Bubble propulsion	Microplastics (personal-care products)	Adsorptive bubble separation	~10% in 2 h	114
Bi_2WO_6	Hydrothermal	~7 μm	Visible light	Textile fibres	Photocatalysis	50 h	115
Fe_3O_4–$BiVO_4$	Hydrothermal	4–8 μm	Visible light and magnetic	Polylactic acid, PCL, PET, polypropylene	Precipitation and photocatalysis	~3% in 7 days	116
Lipase–PDA–Fe_3O_4	Chemical	Micrometre-scale	Magnetic	PCL	Chemical adhesion and enzymatic	24 h	100
Pt–Pd–Fe_2O_3	Hydrothermal and sputtering	3–4 μm	UV light and magnetic	PEG	Electrostatic and photo-Fenton	~100% in 24 h	117
Organic molecules							
OPH-microbead rotifers	Bio-hybrid	100–300 μm	Cilia	Methyl paraoxon	Enzymatic	NR	129
Polypyrrole–Fe_3O_4–Pt	Electrochemical	~10 μm	Bubble propulsion and magnetic	α-Oestradiol	Electrostatic and weaving of macroscopic webs	NR	130
Polyurethane sponge–CFO	Chemical	Millimetre-scale	Bubble propulsion and magnetic	Methylene blue	Fenton-like	90% in 20 min	132
PEDOT–polypyrrole-COOH–Pt	Electrochemical	~10 μm	Bubble propulsion	Dyes	Enzymatic	76–94% in 10 min	134
MIP PINIPAM-Mn_3O_4–$CoFe_2O_4$	Bio-templated	50 μm	Bubble propulsion and magnetic	Erythromycin	Hydrogen bonding and hydrophobic interactions	98% in 1 h	137
Pt–TiO_2 into a 3D-printed robot	3D printing	Millimetre-scale	Marangoni effect	Picric acid	Photocatalysis	6 h	138
Heavy metals							
Pt–nanoclay	Sputtering	~700 nm	Bubble propulsion	Zn^{2+} and Cd^{2+}	Electrostatic	~86% in 5 min	144
Fe_3O_4–MnO_2–MHMs	Biotemplated	~100 μm	Magnetic	Pb^{2+}	Adsorption	99%	147
C_3N_4	Hydrothermal and annealing	50–80 μm	Visible light	Cu^{2+}	Complex formation with N and C functional groups	50% in 7 min	148
Fe_3O_4–Fe–ZIF8-Pt	Chemical	~10 μm	Bubble propulsion and magnetic	UO_2^{2+}	Adsorption	>97% in 1 h	151
MMSNBs	Chemical	~300 nm	Enzymatic and magnetic	Cu^{2+}	Adsorption	80% in 1 h	150
pAsp–Ni–Pt (pCys–Ni–Pt)	Electrochemical	~15 μm	Bubble propulsion and magnetic	Cd^{2+} (CH_3ClHg)	Electrostatic (covalent complex formation)	~100% in 4 min	153
T–T mismatched DNA–Au–Pt	Electrochemical	~10 μm	Bubble propulsion	Hg^{2+}	T–Hg^{2+}–T complex formation	26% in 20 min	154
Pt–MIMs	Chemical and sputtering	~20 μm	Bubble propulsion	^{137}Cs	Adsorption	~99% in 1 h	156
PTBC–TM-Fe_3O_4	Chemical	~200 nm	Magnetic	As	Adsorption	~68% in 100 min	157
nGF–Ni–Pt (Bi–Ni–Pt)	Electrochemical	~12 μm	Bubble propulsion and magnetic	Li^+, Mg^{2+} (Na^+, Ca^{2+})	Intercalation	5 min	158

Table 2 (continued) | Summary of selected micro- and nanorobots for water remediation

Robot	Fabrication method	Size	Motion mechanism	Pollutant	Adsorption and degradation mechanism	Efficiency	Ref.
Oil spills							
Fe_3O_4–Ag–pETPTA	Emulsion	~475 µm	Bubble propulsion	Oil mixture	Hydrophobic interactions	10 min	162
Catalase–Fe_3O_4–PCL	Chemical	~14 µm	Enzymatic and magnetic	Oil mixture	Hydrophobic interactions	~75% in 1 h	163
PDA–Fe_3O_4–PFDT	Chemical	Millimetre-scale	Magnetic	DCM, Chl, toluene	Chemical adhesion	5 min	164
Lipase–MSNPs	Chemical	431 nm	Enzymatic	Tributyrin	Enzymatic	100% in 1 h	165
Microorganisms							
CARs	3D micromoulding	Millimetre-scale	Catalytic and magnetic	Bacterial biofilm	Physical erosion and degradation	NR	174
T-Budbots	Biotemplated	50–160 µm	Magnetic	Bacterial biofilm	Kill-n-clean	50%	109
Iron oxide MHMs	Biotemplated	34 µm	Magnetic	*Escherichia coli*	Photothermal	~99% in 6 min	175
Ag-doped ZnO	Hydrothermal	~5 µm	UV light	Bacterial biofilm	Ag^+ release and photocatalysis	~90% in 5 min	105
$BiVO_4$	Hydrothermal	4–8 µm	Visible light	*Saccharomyces cerevisiae*	Photocatalysis	~40% in 2 h	177
ACE2 algae	Biohybrid	~1 µm	Self-propulsion	SARS-CoV-2 spike protein	Enzymatic	~99% in 16 h	178

ACE2, angiotensin-converting enzyme 2; CAR, catalytic antimicrobial robot; CFO, cobalt ferrite; MHM, magnetic helical microrobot; MIMS, magnetic illite microsphere; MIP, molecularly imprinted polymer; MMSNB, multilayer-sandwich magnetic mesoporous silica nanobottle; MP, microplastic; MSNP, mesoporous silica nanoparticle; nGF, graphite nanofibre; NR, not reported; OPH, organophosphorus hydrolase; pAsp, polyaspartic acid; PCL, polycaprolactone; pCys, polycysteine; PDA, polydopamine; PEDOT, poly(3,4-ethylenedioxythiophene); PEG, polyethylene glycol; PET, polyethylene terephthalate; pETPTA, poly(ethoxylated trimethylolpropane triacylate); PFDT, 1H,1H,2H,2H-perfluorodecanethiol; PNIPAM, poly(N-isopropylacrylamide); PTBC–TM, pluronic tri-block copolymer-thermoresponsive; SPG, sunflower pollen grain; UV, ultraviolet; ZIF, zeolitic imidazolate framework.

on their way, including microplastics extracted from personal-care products and those present in Baltic seawater samples, through phoretic interactions. Moreover, they can assemble into microchains upon exposure to an external magnetic field and move in a coordinated manner. This configuration maximizes the contact area for the capture of microplastics and their removal by shovelling, in this case, by directly pushing them out of the water sample. Similarly, bio-inspired magnetic microrobots made of sunflower pollen grains enable plastic removal on a large scale and at a low cost[113]. These microrobots exhibit three different motion modes (rolling, spinning and wobbling) depending on the applied magnetic field. By tuning the latter, the 'microsubmarines' can cooperate to capture, transport and release a large polystyrene bead (100 µm) or form chains to shovel smaller polystyrene beads owing to the fluid flow generated by their movement.

Adsorptive bubble separation is an alternative approach for the removal of microplastics[114]. This mechanism is based on the bubble propulsion of hydrothermally synthesized Fe_2O_3–MnO_2 core–shell microrobots. Microplastics are trapped in the O_2 bubbles generated by H_2O_2 decomposition during the microrobots' motion. The microplastic-containing bubbles are then pushed toward the solution's surface, creating a foam that can be easily separated. However, the adsorptive bubble separation requires a high H_2O_2 concentration (5%) and a surfactant, and yielded a lower removal efficiency (~10% in 2 h) compared to light-driven Au–Ni–TiO_2 microrobots (67% in 40 s). By contrast, bismuth tungstate (Bi_2WO_6) microrobots swarm under visible light irradiation in 0.025% H_2O_2, attach to textile fibres (a source of microplastic pollution) and destroy them by photocatalysis[115]. This microrobot is particularly advantageous as it does not require expensive metal coatings to move because its motion mechanism is based on asymmetric illumination.

Similar noble-metal-free light-powered and magnetic Fe_3O_4–$BiVO_4$ microrobots have been used to remove and degrade microplastics in a confined space[116]. These microrobots consist of star-shaped microparticles that move under visible light irradiation in 0.1% H_2O_2 as a result of their inherent asymmetry. Their mechanism of action consists of firmly anchoring to large polylactic acid, polycaprolactone (PCL), polyethylene terephthalate (PET) and polypropylene plastic pieces, allowing their transport and removal from a maze of macroscale channels with remarkable efficiencies (~70% for polylactic acid and PCL, ~40% for PET, ~20% for polypropylene in a 10-cm-long hallway). After seven days of exposure to visible light and H_2O_2, the surface chemical and morphological properties of the microplastics start to deteriorate; however, only a poor degradation efficiency (3% for polylactic acid) was estimated as the microplastics' weight loss. Alternatively, PDA-coated Fe_3O_4 microrobots were functionalized with lipase to promote enzymatic degradation of microplastics[100]. Upon actuation by a transversal rotating magnetic field, microrobot swarms adhere to and transport large microplastic pieces (up to 140 µm) owing to PDA's sticky properties. Optical microscopy revealed the enzymatic digestion of PCL microplastics after overnight incubation with the microrobots.

The ultimate goal of plastic sequestration is to completely mineralize the micro- and nanoplastics and their constituent polymer chains into H_2O and CO_2. Micro- and nanorobots can break the strong covalent bonds in polymer chains, as shown by using light-powered Pt–Pd–haematite Janus microrobots[117]. Haematite is a particularly beneficial component because it is a visible-light photoactive semiconductor, a catalyst for Fenton and photo-Fenton reactions and a magnetically

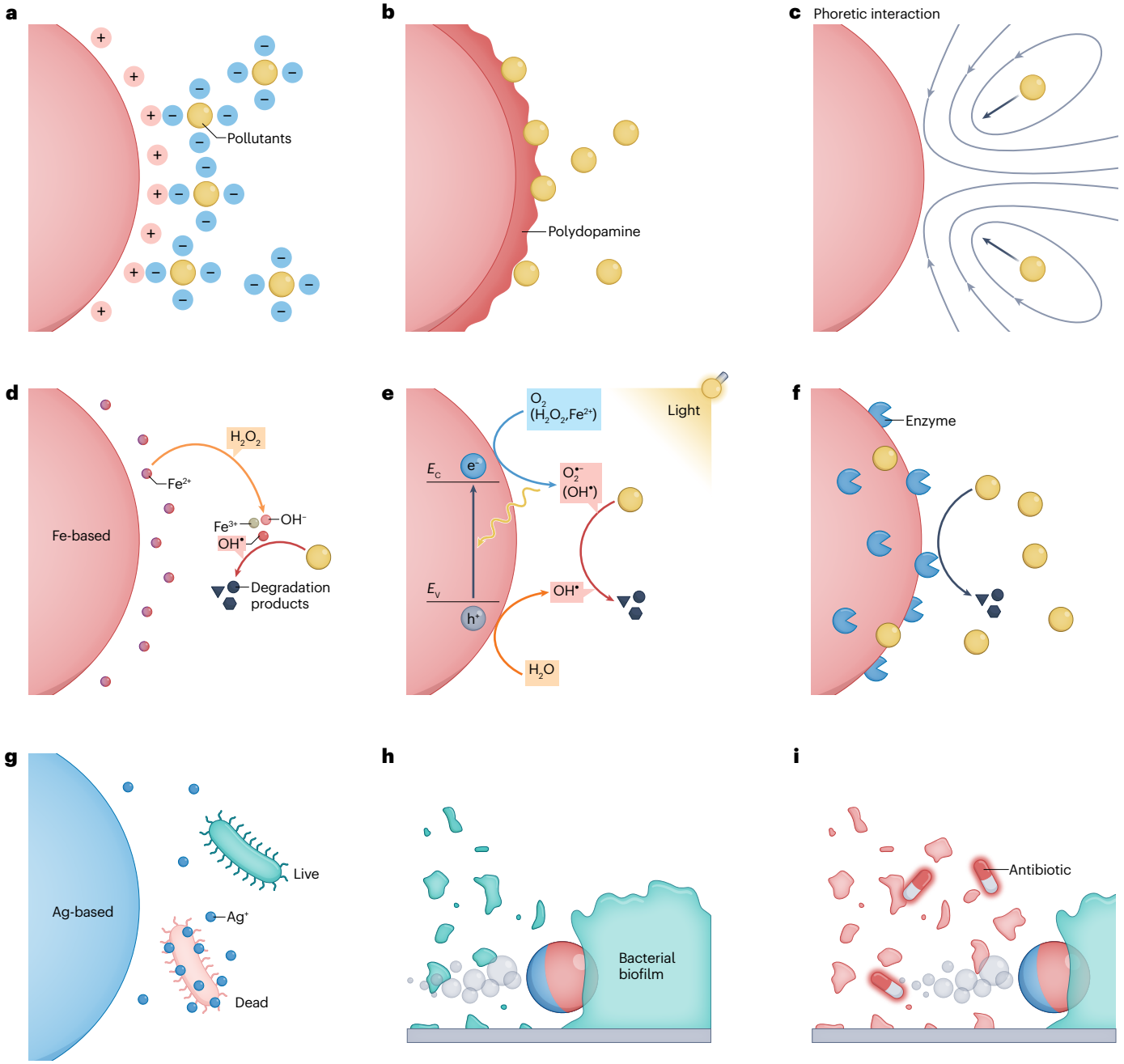

Fig. 4 | Removal and degradation mechanisms of water contaminants by micro- and nanorobots. a, Electrostatic adsorption between the robot's surface and pollutants with opposite surface charge. **b**, Marine-mussel-inspired chemical adhesion of pollutants to a polydopamine-coated robot. **c**, Migration of pollutants toward a robot through phoretic interactions induced by the generated gradients. **d**, Degradation of pollutants by the hydroxyl radicals ($OH^•$) produced by the Fenton reaction between Fe^{2+} ions released from a Fe-based robot and H_2O_2. **e**, Photocatalytic degradation of pollutants owing to reactive oxygen species (ROS) produced by photochemical reactions involving photogenerated electron–hole (e^-–h^+) pairs in a photocatalyst, water and O_2. The photo-Fenton reaction between photogenerated electrons and H_2O_2 further enhances ROS production for iron-oxide-based photocatalysts. **f**, Enzymes immobilized on the robot's surface lower the activation energy necessary to degrade pollutants. **g**, Bacteria killed by the controlled release of bactericidal agents, such as Ag^+, by a Ag-based robot. **h**, Physical erosion of a bacterial biofilm from a surface by a self-propelled robot. **i**, 'Kill-n-clean' approach based on the erosion and complete elimination of a bacterial biofilm from a surface upon release of antibiotics. Removal and degradation strategies are depicted for spherical or bubble-propelled Janus robots, but the concepts can be extended to other classes of micro- and nanorobots. Red and blue hemispheres represent the structural–functional and engine sides of the robot, respectively. E_C, energy level of the conduction band of the semiconductor; E_V, energy level of the valence band of the semiconductor.

navigable material owing to its ferromagnetic properties. These microrobots propel themselves in water and H_2O_2 under light irradiation by self-electrophoresis. The electrostatic attraction between the microrobots and PEG is amplified by adjusting the solution pH, so that at pH 3 the microrobots are positively charged to attract the negatively charged PEG chains. Furthermore, introducing 1% H_2O_2 accelerates the Fenton and photo-Fenton reactions, resulting in total high-molecular-weight polyethylene glycol (PEG) degradation within 24 h. Compared to single-component microrobots, these robots are more expensive because of the noble-metal coating. However, they are more effective owing to the synergy between multiple degradation mechanisms.

Organic molecules

The majority of micro- and nanorobots used for water purification from organic molecules are assessed by their ability to remove or degrade dyes such as methylene blue and rhodamine B[30,118–120]. However, these robots are also effective against more persistent and toxic pollutants, including chemical warfare agents[106], phenolic[121,122] and nitroaromatic compounds[123,124], antibiotics[125,126], hormones[127] and psychoactive substances[128]. Nonetheless, several challenges related to their manufacturing and operational costs and performance (removal or degradation efficiencies, reusability) limit the translation of micro- and nanorobots to real-world settings.

Bio-hybrid microrobots, which combine living microorganisms with synthetic structures, can overcome limitations associated with toxic fuels and expensive noble metal catalysts. For example, self-propelled microrobots based on marine rotifers (microorganisms that live in aquatic environments) have efficiently cleaned the insecticide and nerve agent methyl paraoxon[129], a phosphate triester that is extremely dangerous and difficult to degrade owing to the high chemical stability of its P–O bond. For this purpose, organophosphorus hydrolase (OPH)-functionalized microbeads are accumulated inside the rotifers. The cilia in the rotifers' mouth generate strong fluid flow, which pushes the polluted water toward the microbeads to accelerate the hydrolyzation of the methyl paraoxon into the electrochemically detectable p-nitrophenol, reaching an eightfold increase in degradation efficiency compared to bare OPH-functionalized microbeads. This strategy does not require any fuel and can be extended to other types of contaminants by changing the functional group on the microbeads.

An interesting approach for removing the synthetic hormone α-oestradiol is to use polypyrrole–Fe_3O_4–Pt tubular microrobots. While the inner Pt layer and the Fe_3O_4 nanoparticles enable microrobotic bubble propulsion in H_2O_2 and magnetic steering, respectively, the polypyrrole surface charge can be programmed by adjusting the solution's pH to intensify the electrostatic attraction of the hormone. Surprisingly, once introduced into the α-oestradiol solution, the hormone's adsorption and accumulation on the moving microrobots generates macroscopic spiderweb-like fibres. The microrobots and the woven α-oestradiol webs can then be converted into a single compact piece under an external magnetic field and easily separated from the treated water[130].

The propulsion of micro- and nanorobots enhances fluid mixing, which has been known to accelerate the remediation process. Therefore, it is reasonable to expect that the greater the speed of the micro- and nanorobots, the higher the removal or degradation efficiency. However, a counterintuitive example has been reported, in which light-powered Pt–haematite Janus microrobots with different Pt coating thicknesses degrade picric acid, a model for nitroaromatic explosives, in H_2O_2 by the photo-Fenton reaction[131]. The thicker and more compact Pt coating increases the microrobots' speed at the expense of faster H_2O_2 consumption. Therefore, less H_2O_2 is available for the photo-Fenton reaction, reducing the degradation efficiency. By contrast, in a process termed 'microrobots in sponge', the porous structure of cobalt ferrite microrobots embedded in a polyurethane-based sponge allows more pollutants to be captured, which are then degraded in situ by the microrobots through the Fenton reaction using only 0.13% H_2O_2 (ref. [132]). The microrobots' bubble propulsion enhances fluid mixing and creates a pressure gradient that promotes fluid pumping inside the sponge. The synergy between the properties of the sponge and the microrobots results in methylene blue degradation in large volumes (1 litre in 15 min), allowing the microrobots to be recovered and re-used.

Another strategy aimed at removing organic molecules from water is to digest them enzymatically using laccase[133,134]. Although laccase suffers from loss of enzymatic activity upon exposure to UV light, linking photosensitive azobenzene molecules to microrobots protects enzymes such as horseradish peroxidase, laccase and catalase, enabling enzymatic decomposition of various substrates under direct UV light irradiation[135].

Micro- and nanorobots need to be selective to be able to recognize and treat the most dangerous pollutants in wastewaters. Molecularly imprinted polymers (MIPs) are promising candidates to address this issue. This technique consists of imprinting a molecule (template) on a material (matrix) during its preparation, followed by the template's removal, which leaves complementary cavities that allow selective adsorption of the template[136]. For example, imprinting the antibiotic erythromycin (template) on a thermoresponsive poly(*N*-isopropylacrylamide) (PNIPAM) hydrogel coating (matrix) of Mn_3O_4–$CoFe_2O_4$ microrobots prepared using lotus pollen as a porous bio-template[137] allows MIP-mediated selective recognition and temperature-controlled adsorption and release of erythromycin.

One of the main limitations of micro- and nanorobots for water purification is their short navigation distance (only a few millimetres) when required to operate in large water volumes (cubic metres). Self-propelled 'aircraft-like' carriers of photocatalytic microrobots could solve this problem[138]. For example, a 3D-printed millimetre-scale robot with a conical head and tubular structure filled with ethanol and Pt–TiO_2 microrobots can move for tens of metres by asymmetrically and simultaneously releasing the stored ethanol fuel and the microrobots, a process known as the Marangoni effect. This approach allows the photocatalytic microrobots' slow and distributed release, resulting in picric acid degradation over a large area.

Water-purification studies by micro- and nanorobots are principally conducted using deionized water samples[139]. However, the robots' motion is substantially obstructed or poisoned by solid impurities present in sewage samples, highlighting the need to use real-world specimens in future studies.

Heavy metals

Heavy metals, such as arsenic, cadmium, mercury, lead and copper, are water pollutants of major concern[140]. They tend to accumulate in organisms, causing severe health issues, including metal-induced ROS-mediated oxidative damage[141]. The use of self-propelled micro- and nanorobots is a viable way to remove heavy metals[142,143].

Using natural and abundant materials as the primary building blocks for micro- and nanorobots reduces their fabrication costs. Halloysite nanoclay is an excellent absorber, which forms when rolling

kaolin clay sheet into tubes owing to the strain caused by a lattice mismatch between the adjacent silicon dioxide and aluminum oxide layers over millions of years. Pt-coated nanoclay robots show rapid removal of Zn^{2+} and Cd^{2+} owing to their bubble propulsion in H_2O_2 and electrostatic attraction of the metal cations[144]. Pollen grains are another advantageous material for formulating micro- and nanorobots, owing to their biocompatibility, stability and monodispersity. For example, Pt-covered pollen grains remove Hg^{2+} in H_2O_2 with a remarkable efficiency (~80% in 2 h)[145]. As an alternative to membrane-assisted electrodeposition, kapok fibres can be used as a sacrificial template on which to prepare bubble-propelled tubular microrobots for Cu^{2+} removal[146]. Similarly, spirulina, an edible alga, has been employed as a scaffold on which to fabricate magnetically actuated microrobots, owing to its peculiar helical structure[147]. For example, growing Fe_3O_4 and MnO_2 nanoparticles on spirulina results in swarms of magnetic microrobots that remove Pb^{2+} in H_2O_2-free water under a rotating magnetic field. To reduce dependence on expensive Pt engines, metal-free light-driven C_3N_4 tubular microrobots have been proposed[148]. Under visible-light irradiation, photogenerated carriers in the semiconductor decompose H_2O_2, leading to bubble evolution and self-propulsion. These microrobots remove Cu^{2+} by complex formation with N- and C-based functional groups. Interestingly, the adsorbed metal ions display Fenton-like activity, which increases the decomposition rate of H_2O_2 and, thereby, the speed of the microrobots. Furthermore, this strategy can be extended to capture precious metal ions (Ag^+ and Pd^{2+})[149].

One simple yet effective approach to improve remediation efficiency is to increase the adsorptive area of the micro- and nanorobots. Metal–organic frameworks (MOFs) are attractive materials for this purpose, owing to their large surface area, tuneable pore size and functionalities related to the organic linker, which can be selected according to the targeted application. For example, superstructures with large surface area (~600 $m^2\ g^{-1}$) consisting of asymmetric hollow silica nanobottles, coated with Fe_3O_4 nanoparticles and a catalase-modified mesoporous silica layer, self-propel in H_2O_2, resulting in the rapid removal of Cu^{2+} (80% in 1 h)[150]. Similar MOF-based microrobots can be used to remove metal ions from water, including the radioactive UO_2^{2+} (refs. [151,152]). Another strategy to improve the performance of micro- and nanorobots is to design robots that can selectively remove pollutants. For example, microrobots with a tunable polyaminoacid outer layer selectively eliminate inorganic (Cd^{2+}) or organic (methylmercury) heavy metals, owing to the electrostatic interaction and coordination effect between amino and carboxyl groups in polyaspartic acid and Cd^{2+}, or the stronger bonds between sulfhydryl groups in polycysteine and Hg for methylmercury[153]. Functionalization of Au tubular microrobots with thymine–thymine (T–T) mismatched base pairs is another way to remove Hg^{2+} selectively, preferentially forming the complex T–Hg^{2+}–T (ref. [154]). Similarly, minerals with intrinsic affinity to specific heavy metals can be used to design robots with selective adsorption ability, as in the case of illite and zeolite with the radionuclide Cs^+ (refs. [155,156]).

To be recyclable, micro- and nanorobots must release the captured pollutant in a complete and controlled manner. For example, magnetically actuated nanorobots with thermoresponsive polymeric 'hands' can pick up and dispose of pollutants, including As metal ions, by modulating the water temperature[157]. These nanorobots are made of Fe_3O_4 nanoparticles coated with a pluronic tri-block copolymer formed by a hydrophobic polypropylene oxide core and a thermoresponsive hydrophilic polyethylene oxide shell. Exposure to 5 mg per litre As for 100 min in water at 25 °C under a rotating magnetic field results in 65% pickup efficiency, followed by a disposal efficiency of 48% in water at 5 °C. After ten cycles, these efficiencies drop slightly to 38% and 31% for pickup and disposal, respectively.

Inspired by the supercapacitors' charge storage mechanism, graphite nanofibre–Ni–Pt or Bi–Ni–Pt bubble-propelled tubular microrobots can also be used for the selective electroadsorption of heavy metals[158]. Upon collision with a negatively charged electrode, electrons are transferred to the microrobots, allowing the adsorption of the metal cations by electrostatic forces in an O_2-free solution. Unlike previous examples, adsorption is not limited to the microrobots' surface, but includes the layered structure of graphite and Bi to intercalate the metal cations in the interlayer spacing up to ~400 layers from the microrobots' surface. Furthermore, owing to their different interlayer distance, graphite-based microrobots selectively capture Li^+, whereas Bi-based microrobots removed larger cations such as Na^+ and Ca^{2+}. By magnetically transferring the microrobots to an O_2-saturated solution, the cations are promptly released, allowing their multiple use.

Oil spills

The increase in tanker operations with the associated leakage of petroleum and other oil spills into water bodies (and lack of suitable discharge thereof), has become a substantial environmental problem[159]. Oil release counts for more than one million metric tons per year, calling for urgent and practical solutions. One of the first examples of micro- and nanorobots used for oil remediation involved Au–Ni–poly(3,4-ethylenedioxythiophene) (PEDOT)–Pt microtubes modified with a self-assembled monolayer of long alkanethiol chains[160]. Owing to their strong hydrophobic interactions with oil droplets, the microrobots capture and transport oil spills in H_2O_2. Replacing Pt and H_2O_2 with a disintegrating engine reduces the cost and toxicity of microrobots at the expense of their lifetime[161]. Therefore, new fabrication and propulsion methods have been proposed to develop hydrophobic microrobots. For example, tuning the evolution of microfluidic double emulsions asymmetrically loaded with Fe_3O_4–Ag nanoparticles results in hierarchically porous polymeric spheres containing two microscale pores in a nanoporous matrix[162]. The nanoparticles ensure powerful bubble propulsion in H_2O_2 (~1,600 μm s^{-1}) while capturing oil, and magnetic collectability to enable the washing and re-use of the microrobots. Similarly, walnut-like microrobots composed of PCL, Fe_3O_4 nanoparticles and catalase have been fabricated through a one-step electrospinning process[163]. The microrobots move by catalase-induced bubble propulsion in H_2O_2, assisted by the photothermal effect produced by the Fe_3O_4 nanoparticles under light irradiation, whereas the PCL hydrophobic surface ensures the adsorption of spilled oil.

Magnetically powered micro- and nanorobots have emerged in oil removal owing to their effective and environmentally friendly actuation mode. For example, 3D porous magnetic oil collectors formulated by modifying a commercial polyurethane sponge with PDA nanoparticles, can be used as a navigable bifunctional platform on which to link Fe_3O_4 nanoparticles and 1H,1H,2H,2H-perfluorodecanethiol (PFDT), changing the sponge's wettability from hydrophilic to superhydrophobic[164]. Similarly, magnetic microsubmarines based on sunflower pollen grains can move at the liquid–liquid interface (water–oil) and the liquid–solid interface (the bottom of the vessel)[113]. The highly ordered nanospikes and super-oleophilicity of the microsubmarines enable adsorption and transport of oil droplets 37 times larger than their own volume.

In these examples, the removed oil spills were not completely degraded. To overcome this issue, enzyme-modified bio-inspired nanorobots have been proposed for the in situ degradation of oils.

For example, using triacetin as fuel, mesoporous silica nanoparticles decorated with lipase obtained from *Candida rugosa* decompose dissolvable and slightly dissolvable triglyceride substrates, a model for oil pollutants[165]. Interestingly, the enzyme undergoes conformational changes depending on the different orientation and accessibility of the catalytic centre[166]. Furthermore, designing lipase-modified nanorobots in a yolk@spiky–shell structure endowed with near-infrared light responsiveness allows precise navigation towards oil droplets, showing a high degradation efficiency of ~90% in 20 min owing to the synergistic combination of enzymatic and photothermal mechanisms[167].

Microorganisms

Biological pollution in water arises from pathogenic microorganisms like viruses, bacteria, fungi and protozoa[168]. These pathogens pose severe risks for humans and animals, causing large-scale morbidity and mortality. Microorganisms can adapt to their surroundings, switch to a dormant state in which they can survive for extended periods without nutrients and resume proliferation under favourable conditions. Furthermore, they release toxins as secondary metabolites and acquire resistance to decontaminants, hindering their complete removal[169]. Contamination of aquatic resources is mostly of faecal origin, which spreads owing to poor water quality, lack of sanitation and inadequate hygiene[170]. Current disinfection methods are based on UV treatments and chlorine, chloramines or ozone[171]. However, these processes consume a substantial amount of energy (UV treatment), produce harmful by-products and require high doses of disinfectants to avoid pathogenic recolonization, a treatment that favours the establishment of resistant microbial biofilms. Furthermore, the effectiveness of traditional disinfection techniques against new fungal, bacterial and viral species is unknown and must be evaluated to avoid future outbreaks[172].

The first attempts to remove aqueous pathogens focused on killing bacteria 'on the fly' by modifying microrobots with anti-bactericidal agents such as antibiotics, enzymes, protein receptors and metal ions[173]. However, bacterial biofilms preferentially grow in inaccessible locations, which requires the ability to control the movement of robots through, for example, using an external magnetic field. In this regard, catalytic antimicrobial robots (CARs) that incorporate iron oxide nanoparticles have been designed to remove bacterial biofilm grown at the end of conical tubings, mimicking a clogging plaque[174]. Exposing helicoidal CARs to H_2O_2, mutanase–dextranase enzyme solution and a rotating magnetic field prompts CARs to rapidly move in a corkscrew-like fashion (5 mm s^{-1}), resulting in biofilm matrix drilling and removal. Simultaneously, the catalytic action of CARs removes the remaining biofilm clogs by killing all bacterial debris, thereby avoiding regrowth. Persistent bacterial biofilms can also be removed using the 'kill-n-clean' method (Fig. 4i). For example, magnetic microrobots derived from biocompatible porous tea buds, loaded with ciprofloxacin and decorated with Fe_3O_4 nanoparticles, exploit the acidic microenvironment of bacterial biofilms to release antibiotics in a pH-dependent manner, resulting in the simultaneous eradication and degradation of the biofilm[109]. Similarly, magnetically actuated helical microswimmers with an inner carbon core synergistically combine light and magnetic fields to kill *E. coli* bacteria through a photothermal effect under near-infrared light irradiation[175].

Light-propelled micro- and nanorobots are another valuable solution for eliminating bacterial biofilms. These robots can move and simultaneously generate ROS, inducing substantial damage to the biofilm and preventing its regrowth. For example, intrinsically asymmetric Ag-doped ZnO microrobots demonstrate autonomous motion under UV light irradiation while destroying gram-negative *Pseudomonas aeruginosa* and gram-positive methicillin-resistant *Staphylococcus aureus* (MRSA) bacterial biofilms with higher efficiency (~50% in 5 min) than in the static condition without light irradiation (~10% in 5 min), as indicated by live–dead assay[105]. To avoid using UV light, bactericidal nanorobots consisting of Ag-coated TiO_2 nanotubes allow eradication of multispecies bacterial biofilms firmly attached to metallic surfaces (40% efficiency in 30 min). Owing to their broad light absorption from the UV to the visible region, these nanorobots vary in speed and motion type, resulting in modes such as clock-like rotation (up to 500 rpm) and swimming along random trajectories (30 μm s^{-1})[176]. Interestingly, upon visible light exposure, star-shaped light-powered $BiVO_4$ microrobots generate chemical gradients that allow them to swim and assemble into swarms to capture and kill fungal microbes (*Saccharomyces cerevisiae*) in water, rendering them photocatalytically inactivated[177].

To remove pathogens on a large scale, biohybrid robots can be used[178]. For example, self-motile *Chlamydomonas reinhardtii* microalgae, covalently bound to the angiotensin-converting enzyme 2 (ACE2) receptor through a click-chemistry reaction, efficiently remove the SARS-CoV-2 viral spike protein (95%) and pseudovirus (89%). Moreover, these biohybrid microbots display fast (>100 μm s^{-1}) and long-lasting motion (24 h) and reusability for five consecutive cycles in different water matrices, including acetate phosphate medium, phosphate-buffered saline, drinking water and river water, without needing fuel.

Outlook

Self-propulsion has provided micro- and nanomaterials with an additional engineering dimension, allowing the development of swarms of intelligent small-scale robots that move in response to external stimuli and cooperate to accomplish selected tasks. For water-remediation applications, where the efficacy and speed of the purification process are crucial, micro- and nanorobots have proved effective owing to the synergy between active motion and programmable pollutant removal–degradation mechanisms through material design. Despite the breadth of efficacy of micro- and nanorobots against contaminants differing in nature and size (millimetre- to atomic-scale), several challenges must still be faced for real-world applications.

The main limitation is related to their applicability in open-water bodies such as oceans, seas, lakes and rivers. In principle, fuel-free sunlight-powered micro- and nanorobots are suitable for offshore water treatment because their activation does not require expensive and bulky apparatus (as for the magnetic actuation) or a chemical fuel that would be dispersed in an open space. However, their propulsion might be hindered by the decreasing light penetration with depth, restricting their use to surface-water treatment. Moreover, the motility of light-driven self-electrophoretic robots is hampered in high-salinity waters owing to the higher solution conductivity, which decreases the autogenerated electric field[179]. In addition, marine currents could overcome the motion of the robots, impeding their recovery and re-use. Alternatively, micro- and nanorobots can be actuated in a confined space (for example, a tub or tank), constraining potential secondary pollution phenomena (Box 1). Providing sufficient light intensity over the whole water volume using additional light sources could simultaneously sustain robotic movement and pollutant removal and degradation. 'Hybrid' robots exploiting multiple motion modes could further improve water-purification performance. For example, chemical fuels and electric fields can be used to boost the speed of light-driven robots[180]. Alternatively, magnetic fields allow us to control swarms of robots whose propulsion is not affected by the properties

Box 1

Robot-based water-remediation systems

Micro- and nanorobots are not suitable for remediation of open-water bodies (such as oceans), but can be used to remove or degrade contaminants in confined spaces, for example, by integration onboard a ship for offshore operations. Any small-scale robot-based water-remediation system should include a tank with an inlet pipe for contaminated water and an outlet pipe for clean water, equipped with sensors to assess post-treatment water quality (see the figure). The tank can be exposed to direct sunlight or arrays of ultraviolet lights to power light-driven robots, with the assistance of H_2O_2 fuel if necessary. However, magnetic actuation might be preferred over light-driven actuation, especially for salty water where the high conductivity reduces the self-generated electric field that enables the movement of most light-driven micro- and nanorobots. Therefore, the tank could also be surrounded by a set of orthogonal magnetic coil pairs directed by the operator through an external controller. This system facilitates the movement of the robots to accelerate the adsorption (or degradation) of the pollutants and for collecting the robots at a preset location at the end of the treatment to let purified water exit. Moreover, magnetic actuation can be used to direct robots toward a second vessel where non-degradable pollutants can be controllably released, enabling re-use of the robots. Therefore, an ideal micro- or nanorobot must include several components with specific functions to meet these technical requirements (see the figure). For example, it could contain a magnetic engine as the core to ensure control over its location, speed and trajectory by regulating the magnetic field parameters. The engine could be surrounded by an adsorber with a large surface area (for example, a highly porous material) to maximize adsorption efficiency. The adsorber can be, in turn, coated by a shell of a photoresponsive material capable of undergoing one or multiple photodegradation pathways. If necessary, the robots' surface can be further functionalized with enzymes to facilitate pollutants' decomposition thereby boosting degradation efficiency[181]. Importantly, enzymes' stability under exposure to light and photo-generated reactive oxygen species (ROS) needs to be evaluated. Such a system must be environmentally safe, with competitive production costs compared to conventional drinking-water distribution systems. In addition, a complete economic assessment of a system similar to the one described here should consider the energy consumption of pumping water, sensors to monitor the water quality, the controller of the magnetic setup, light sources and, importantly, the exact treatment duration. These parameters depend on the removal efficiency, which, in turn, is a function of other variables, including the nature of the pollutant, the number of robots, the parameters of the magnetic field and the light intensity.

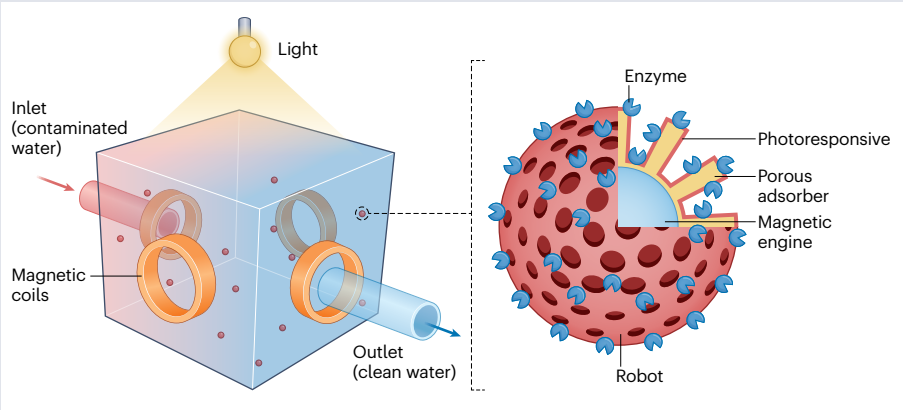

of the medium, such as its conductivity, after which fuels and light might be required to degrade the removed pollutants. Such a system must ensure a more efficient, safer and cheaper operation than current water-purification plants before it can be commercialized. Accordingly, for a proper estimation of production efficiency, quality, robustness and costs, the energy consumption associated with micro- and nanorobot operation must also be evaluated (Box 1).

Self-propelled micro- and nanorobots are more efficient than static materials for water-remediation applications. Furthermore, the removal and degradation efficiency is not satisfactory for all the pollutants investigated. For example, achieving total decomposition of plastic waste is particularly challenging, because plastics contain UV stabilizers to improve their stability. One practical solution is to combine multiple degradation mechanisms in the same robot or to program it to target the most persistent contaminant selectively. These features require the integration of multiple components, resulting in higher complexity and production costs. Therefore, the design of micro- and nanorobots must be kept as simple as possible while meeting the requirements of mass production, such as by using high-throughput fabrication methods (for example, 3D bioprinting). An associated risk to take into account is the accumulation of small-scale robots in the environment. In this context, using abundant, biocompatible and biodegradable natural materials such as microalgae is an attractive option.

Micro- and nanorobots can also be used to remediate soil and plants, which are at great risk of contamination owing to the extensive application of toxic pesticides in agriculture to improve crop yield. Environmentally friendly and biocompatible small-scale robots could decompose pesticides into harmless products in situ. As in water remediation, the robots need a liquid medium to facilitate their active movement and to enable removal and degradation of contaminants. One strategy could be to suspend the robots in water sprayed on the soil or plants' surface, degrading the pesticides at the water–soil and water–plant interfaces under sunlight. Alternatively, they can be designed to target pests directly, thereby replacing the role of toxic pesticides.

Numerous studies have proved the immense potential of using micro- and nanorobots for water remediation. However, translation of this technology to real-world applications needs the combined efforts of scientists from different backgrounds, including physicists, chemists, biologists and engineers, to meet market demands.

Published online: 6 February 2023

References

1. Favere, J. et al. Safeguarding the microbial water quality from source to tap. *npj Clean Water* **4**, 28 (2021).
2. Wu, J., Cao, M., Tong, D., Finkelstein, Z. & Hoek, E. M. V. A critical review of point-of-use drinking water treatment in the United States. *npj Clean Water* **4**, 40 (2021).
3. Werber, J. R., Osuji, C. O. & Elimelech, M. Materials for next-generation desalination and water purification membranes. *Nat. Rev. Mater.* **1**, 16018 (2016).
4. Nguyen, P. Y., Carvalho, G., Reis, M. A. M. & Oehmen, A. A review of the biotransformations of priority pharmaceuticals in biological wastewater treatment processes. *Water Res.* **188**, 116446 (2021).
5. Liu, S. et al. Understanding, monitoring, and controlling biofilm growth in drinking water distribution systems. *Environ. Sci. Technol.* **50**, 8954–8976 (2016).
6. Berendonk, T. U. et al. Tackling antibiotic resistance: the environmental framework. *Nat. Rev. Microbiol.* **13**, 310–317 (2015).
7. Salzano de Luna, M. Recent trends in waterborne and bio-based polyurethane coatings for corrosion protection. *Adv. Mater. Interfaces* **9**, 2101775 (2022).
8. Song, Y., Mukasa, D., Zhang, H. & Gao, W. Self-powered wearable biosensors. *Acc. Mater. Res.* **2**, 184–197 (2021).
9. Mestre, R., Patiño, T. & Sánchez, S. Biohybrid robotics: from the nanoscale to the macroscale. *Wiley Interdisc. Rev. Nanomed. Nanobiotech.* **13**, e1703 (2021).
10. Ussia, M. & Pumera, M. Towards micromachine intelligence: potential of polymers. *Chem. Soc. Rev.* **51**, 1558–1572 (2022).
This article reviews polymeric materials that enable the formulation of nature-mimicking micromachine intelligentization.
11. Tan, L., Davis, A. C. & Cappelleri, D. J. Smart polymers for microscale machines. *Adv. Funct. Mater.* **31**, 2007125 (2021).
12. Soto, F. et al. Smart materials for microrobots. *Chem. Rev.* **122**, 5365–5403 (2021).
This Review provides an overview of smart responsive materials for formulating self-propelled, biocompatible, cooperative and intelligent microrobots.
13. Li, M., Pal, A., Aghakhani, A., Pena-Francesch, A. & Sitti, M. Soft actuators for real-world applications. *Nat. Rev. Mater.* **7**, 235–249 (2022).
14. Pané, S., Wendel-Garcia, P., Belce, Y., Chen, X.-Z. & Puigmartí-Luis, J. Powering and fabrication of small-scale robotics systems. *Curr. Robot. Rep.* **2**, 427–440 (2021).
15. Palagi, S. & Fischer, P. Bioinspired microrobots. *Nat. Rev. Mater.* **3**, 113–124 (2018).
16. Wang, J. Can man-made nanomachines compete with nature biomotors? *ACS Nano* **3**, 4–9 (2009).
17. Mallouk, T. E. & Sen, A. Powering nanorobots. *Sci. Am.* **300**, 72–77 (2009).
18. Zhang, Y., Yuan, K. & Zhang, L. Micro/nanomachines: from functionalization to sensing and removal. *Adv. Mater. Technol.* **4**, 1800636 (2019).
19. Karshalev, E., Esteban-Fernández De Ávila, B. & Wang, J. Micromotors for 'chemistry-on-the-fly'. *J. Am. Chem. Soc.* **140**, 3810–3820 (2018).
20. Wang, B., Kostarelos, K., Nelson, B. J. & Zhang, L. Trends in micro-/nanorobotics: materials development, actuation, localization, and system integration for biomedical applications. *Adv. Mater.* **33**, 2002047 (2021).
21. Zhu, S. et al. External field-driven untethered microrobots for targeted cargo delivery. *Adv. Mater. Technol.* **7**, 2101256 (2021).
22. Jurado-Sánchez, B., Campuzano, S., Pingarrón, J. M. & Escarpa, A. Janus particles and motors: unrivaled devices for mastering (bio)sensing. *Microchim. Acta* **188**, 416 (2021).
23. Venugopalan, P. L., Esteban-Fernández De Ávila, B., Pal, M., Ghosh, A. & Wang, J. Fantastic voyage of nanomotors into the cell. *ACS Nano* **14**, 9423–9439 (2020).
24. Schmidt, C. K., Medina-Sánchez, M., Edmondson, R. J. & Schmidt, O. G. Engineering microrobots for targeted cancer therapies from a medical perspective. *Nat. Commun.* **11**, 5618 (2020).
25. Yuan, K., Bujalance-Fernández, J., Jurado-Sánchez, B. & Escarpa, A. Light-driven nanomotors and micromotors: envisioning new analytical possibilities for bio-sensing. *Microchim. Acta* **187**, 187–581 (2020).
26. Huang, T.-Y., Gu, H. & Nelson, B. J. Increasingly intelligent micromachines. *Annu. Rev. Control Robot. Auton. Syst.* **5**, 279–312 (2022).
27. Wang, H. & Pumera, M. Fabrication of micro/nanoscale motors. *Chem. Rev.* **115**, 8704–8735 (2015).
28. Men, Y., Peng, F. & Wilson, D. A. Micro/nanomotors via self-assembly. *Sci. Lett. J.* **5**, 219 (2016).
29. Wu, Z., Lin, X., Si, T. & He, Q. Recent progress on bioinspired self-propelled micro/nanomotors via controlled molecular self-assembly. *Small* **12**, 3080–3093 (2016).
30. Shivalkar, S. et al. Autonomous magnetic microbots for environmental remediation developed by organic waste derived carbon dots. *J. Environ. Manage.* **297**, 113322 (2021).
31. Fernández-Medina, M., Ramos-Docampo, M. A., Hovorka, O., Salgueiriño, V. & Städler, B. Recent advances in nano- and micromotors. *Adv. Funct. Mater.* **30**, 1908283 (2020).
32. Soler, L. & Sánchez, S. Catalytic nanomotors for environmental monitoring and water remediation. *Nanoscale* **6**, 7175–7182 (2014).
33. Dey, K. K., Wong, F., Altemose, A. & Sen, A. Catalytic motors — quo vadimus? *Curr. Opin. Colloid Interface Sci.* **21**, 4–13 (2016).
34. Wilson, D. A., Nolte, R. J. M. & Van Hest, J. C. M. Autonomous movement of platinum-loaded stomatocytes. *Nat. Chem.* **4**, 268–274 (2012).
35. Tu, Y. et al. Self-propelled supramolecular nanomotors with temperature-responsive speed regulation. *Nat. Chem.* **9**, 480–486 (2017).
36. Moran, J. & Posner, J. Microswimmers with no moving parts. *Phys. Today* **72**, 44–50 (2019).
37. Li, J., Rozen, I. & Wang, J. Rocket science at the nanoscale. *ACS Nano* **10**, 5619–5634 (2016).
38. Urso, M., Iffelsberger, C., Mayorga-Martinez, C. C. & Pumera, M. Nickel sulfide microrockets as self-propelled energy storage devices to power electronic circuits "on-demand". *Small Methods* **5**, 2100511 (2021).
39. Mathesh, M., Sun, J. & Wilson, D. A. Enzyme catalysis powered micro/nanomotors for biomedical applications. *J. Mater. Chem. B* **8**, 7319–7334 (2020).
40. Yang, Q. et al. Enzyme-driven micro/nanomotors: recent advances and biomedical applications. *Int. J. Biol. Macromol.* **167**, 457–469 (2021).
41. Yuan, H., Liu, X., Wang, L. & Ma, X. Fundamentals and applications of enzyme powered micro/nano-motors. *Bioact. Mater.* **6**, 1727–1749 (2021).
42. Hortelao, A. C. et al. Swarming behavior and in vivo monitoring of enzymatic nanomotors within the bladder. *Sci. Robot.* **6**, eabd2823 (2021).
43. Liu, K. et al. Magnesium-based micromotors for enhanced active and synergistic hydrogen chemotherapy. *Appl. Mater. Today* **20**, 100694 (2020).
44. Yang, J. et al. γ-Fe_2O_3@Ag-mSiO_2_NH_2 magnetic Janus micromotor for active water remediation. *Appl. Mater. Today* **25**, 101190 (2021).
45. Nourhani, A., Karshalev, E., Soto, F. & Wang, J. Multigear bubble propulsion of transient micromotors. *Research* **2020**, 7823615 (2020).
46. Gao, Y., Xiong, Z., Wang, J., Tang, J. & Li, D. Light hybrid micro/nano-robots: from propulsion to functional signals. *Nano Res.* **15**, 5355–5375 (2022).
47. Zhou, D., Zhuang, R., Chang, X. & Li, L. Enhanced light-harvesting efficiency and adaptation: a review on visible-light-driven micro/nanomotors. *Research* **2020**, 6821595 (2020).
48. Villa, K. & Pumera, M. Fuel-free light-driven micro/nanomachines: artificial active matter mimicking nature. *Chem. Soc. Rev.* **48**, 4966–4978 (2019).
49. Kong, L., Mayorga-Martinez, C. C., Guan, J. & Pumera, M. Photocatalytic micromotors activated by UV to visible light for environmental remediation, micropumps, reversible assembly, transportation, and biomimicry. *Small* **16**, 1903179 (2020).
50. Oral, C. M., Ussia, M., Yavuz, D. K. & Pumera, M. Shape engineering of TiO_2 microrobots for "on-the-fly" optical brake. *Small* **18**, 2106271 (2022).
51. Wu, Y., Dong, R., Zhang, Q. & Ren, B. Dye-enhanced self-electrophoretic propulsion of light-driven TiO_2–Au Janus micromotors. *Nanomicro Lett.* **9**, 30 (2017).
52. Chattopadhyay, P., Heckel, S., Pereira, F. I. & Simmchen, J. A path toward inherently asymmetric micromotors. *Adv. Intell. Syst.* 2200091 (2022).
53. Chen, X. Z. et al. Recent developments in magnetically driven micro- and nanorobots. *Appl. Mater. Today* **9**, 37–48 (2017).
54. Zhou, H., Mayorga-Martinez, C. C., Pané, S., Zhang, L. & Pumera, M. Magnetically driven micro and nanorobots. *Chem. Rev.* **121**, 4999–5041 (2021).
55. Wang, X. et al. MOFBOTS: metal–organic-framework-based biomedical microrobots. *Adv. Mater.* **31**, 1901592 (2019).
56. Sitti, M. & Wiersma, D. S. Pros and cons: magnetic versus optical microrobots. *Adv. Mater.* **32**, 1906766 (2020).
57. Yang, Q. et al. Recent advances in motion control of micro/nanomotors. *Adv. Intell. Syst.* **2**, 2000049 (2020).
58. Li, J., Mayorga-Martinez, C. C., Ohl, C. D. & Pumera, M. Ultrasonically propelled micro- and nanorobots. *Adv. Funct. Mater.* **32**, 2102265 (2022).
59. Rao, K. J. et al. A force to be reckoned with: a review of synthetic microswimmers powered by ultrasound. *Small* **11**, 2836–2846 (2015).
60. Xu, T., Xu, L. P. & Zhang, X. Ultrasound propulsion of micro-/nanomotors. *Appl. Mater. Today* **9**, 493–503 (2017).
61. Li, D. et al. Single-metal hybrid micromotor. *Front. Bioeng. Biotechnol.* **10**, 844328 (2022).
62. Esteban-Fernández De Ávila, B. et al. Acoustically propelled nanomotors for intracellular siRNA delivery. *ACS Nano* **10**, 4997–5005 (2016).
63. Esteban-Fernández De Ávila, B. et al. Single cell real-time miRNAs sensing based on nanomotors. *ACS Nano* **9**, 6756–6764 (2015).
64. Yang, J. et al. Three-dimensional hierarchical HRP-MIL-100(Fe)@TiO_2@Fe_3O_4 Janus magnetic micromotor as a smart active platform for detection and degradation of hydroquinone. *ACS Appl. Mater. Interfaces* **14**, 6484–6498 (2022).
65. Huang, Y. et al. Magnetic-controlled dandelion-like nanocatalytic swarm for targeted biofilm elimination. *Nanoscale* **14**, 6497–6506 (2022).
66. Muñoz, J., Urso, M. & Pumera, M. Self-propelled multifunctional microrobots harboring chiral supramolecular selectors for "enantiorecognition-on-the-fly". *Angew. Chem. Int. Ed.* **61**, e202116090 (2022).
67. Li, Y. et al. Biohybrid bacterial microswimmers with metal–organic framework exoskeletons enable cytoprotection and active drug delivery in a harsh environment. *Mater. Today Chem.* **23**, 100609 (2022).
68. Urso, M. & Pumera, M. Micro- and nanorobots meet DNA. *Adv. Funct. Mater.* **32**, 2200711 (2022).

69. Wang, J. Will future microbots be task-specific customized machines or multi-purpose "all in one" vehicles? *Nat. Commun.* **12**, 7125 (2021).
70. Mattingly, H. H., Kamino, K., Machta, B. B. & Emonet, T. *Escherichia coli* chemotaxis is information limited. *Nat. Phys.* **17**, 1426–1431 (2021).
71. Giometto, A., Altermatt, F., Maritan, A., Stocker, R. & Rinaldo, A. Generalized receptor law governs phototaxis in the phytoplankton *Euglena gracilis*. *Proc. Natl Acad. Sci. USA* **112**, 7045–7050 (2015).
72. Gao, C., Feng, Y., Wilson, D. A., Tu, Y. & Peng, F. Micro–nano motors with taxis behavior: principles, designs, and biomedical applications. *Small* **18**, 2106263 (2022).
73. You, M., Chen, C., Xu, L., Mou, F. & Guan, J. Intelligent micro/nanomotors with taxis. *Acc. Chem. Res.* **51**, 3006–3014 (2018).
74. Ye, Y. et al. Apoptotic tumor DNA activated nanomotor chemotaxis. *Nano Lett.* **21**, 8086–8094 (2021).
75. Xu, D. et al. Enzyme-powered liquid metal nanobots endowed with multiple biomedical functions. *ACS Nano* **15**, 11543–11554 (2021).
76. Frank, B. D., Baryzewska, A. W., Giusto, P., Seeberger, P. H. & Zeininger, L. Reversible morphology-resolved chemotactic actuation and motion of Janus emulsion droplets. *Nat. Commun.* **13**, 2562 (2022).
77. Cao, S. et al. Photoactivated nanomotors via aggregation induced emission for enhanced phototherapy. *Nat. Commun.* **12**, 2077 (2021).
78. Lin, G. et al. Programmable phototaxis of metal–phenolic particle microswimmers. *Adv. Mater.* **33**, 2006177 (2021).
79. He, X. et al. Dipole-moment induced phototaxis and fuel-free propulsion of ZnO/Pt Janus micromotors. *Small* **17**, 2101388 (2021).
80. Dai, B. et al. Programmable artificial phototactic microswimmer. *Nat. Nanotechnol.* **11**, 1087–1092 (2016).
81. Zhang, J. et al. Photochemical micromotor of eccentric core in isotropic hollow shell exhibiting multimodal motion behavior. *Appl. Mater. Today* **26**, 101371 (2022).
82. Zhou, C., Zhang, H. P., Tang, J. & Wang, W. Photochemically powered AgCl Janus micromotors as a model system to understand ionic self-diffusiophoresis. *Langmuir* **34**, 3289–3295 (2018).
83. Urso, M., Ussia, M., Novotný, F. & Pumera, M. Trapping and detecting nanoplastics by MXene-derived oxide microrobots. *Nat. Commun.* **13**, 3573 (2022).
This article describes an example of tactic robots where photogravitactic MXene-derived microrobots electrochemically detect and mop up nanoplastics in the 3D space.
84. Huang, H. W. et al. Investigation of magnetotaxis of reconfigurable micro-origami swimmers with competitive and cooperative anisotropy. *Adv. Funct. Mater.* **28**, 1802110 (2018).
85. Santomauro, G. et al. Incorporation of terbium into a microalga leads to magnetotactic swimmers. *Adv. Biosyst.* **2**, 1800039 (2018).
86. Li, Q. et al. Nanoparticle-regulated semiartificial magnetotactic bacteria with tunable magnetic moment and magnetic sensitivity. *Small* **15**, 1900427 (2019).
87. Wang, H. & Pumera, M. Coordinated behaviors of artificial micro/nanomachines: from mutual interactions to interactions with the environment. *Chem. Soc. Rev.* **49**, 3211–3230 (2020).
88. Yang, L. et al. Autonomous environment-adaptive microrobot swarm navigation enabled by deep learning-based real-time distribution planning. *Nat. Mach. Intell.* **4**, 480–493 (2022).
89. Zhang, J. et al. Cooperative transport by flocking phototactic micromotors. *Nanoscale Adv.* **3**, 6157–6163 (2021).
90. Chen, Z. et al. Visible light-regulated $BiVO_4$-based micromotor with biomimetic 'predator-bait' behavior. *J. Mater. Sci.* **57**, 4092–4103 (2022).
91. Shen, Y. et al. Adaptive control of nanomotor swarms for magnetic-field-programmed cancer cell destruction. *ACS Nano* **15**, 20020–20031 (2021).
92. Yue, H., Chang, X., Liu, J., Zhou, D. & Li, L. Wheel-like magnetic-driven microswarm with a band-aid imitation for patching up microscale intestinal perforation. *ACS Appl. Mater. Interfaces* **14**, 8743–8752 (2022).
93. Lu, X. et al. Universal control for micromotor swarms with a hybrid sonoelectrode. *Small* **17**, 2104516 (2021).
94. Peng, X., Urso, M., Ussia, M. & Pumera, M. Shape-controlled self-assembly of light-powered microrobots into ordered microchains for cells transport and water remediation. *ACS Nano* **16**, 7615–7625 (2022).
95. Gardi, G., Ceron, S., Wang, W., Petersen, K. & Sitti, M. Microrobot collectives with reconfigurable morphologies, behaviors, and functions. *Nat. Commun.* **13**, 2239 (2022).
96. Huang, L., Moran, J. L. & Wang, W. Designing chemical micromotors that communicate — a survey of experiments. *JCIS Open.* **2**, 100006 (2021).
97. Cheng, Y. et al. Long-range hydrodynamic communication among synthetic self-propelled micromotors. *Cell Rep. Phys. Sci.* **3**, 100739 (2022).
98. Urso, M. & Pumera, M. Nano/microplastics capture and degradation by autonomous nano/microrobots: a perspective. *Adv. Funct. Mater.* **32**, 2112120 (2022).
99. Shivalkar, S., Gautam, P. K., Chaudhary, S., Samanta, S. K. & Sahoo, A. K. Recent development of autonomously driven micro/nanobots for efficient treatment of polluted water. *J. Environ. Manage.* **281**, 111750 (2021).
100. Zhou, H., Mayorga-Martinez, C. C. & Pumera, M. Microplastic removal and degradation by mussel-inspired adhesive magnetic/enzymatic microrobots. *Small Methods* **5**, 2100230 (2021).
101. Wang, L., Kaeppler, A., Fischer, D. & Simmchen, J. Photocatalytic TiO_2 micromotors for removal of microplastics and suspended matter. *ACS Appl. Mater. Interfaces* **11**, 32937–32944 (2019).
102. Ameta, S. C. in *Advanced Oxidation Processes For Wastewater Treatment: Emerging Green Chemical Technology* (eds Ameta, S. & Ameta, R.) 1–13 (Elsevier, 2018).
103. Glaze, W. H., Kang, J. W. & Chapin, D. H. The chemistry of water treatment processes involving ozone, hydrogen peroxide and ultraviolet radiation. *Ozone Sci. Eng.* **9**, 335–352 (1987).
104. Kumar, L. & Bharadvaja, N. Ein *Smart Bioremediation Technologies: Microbial Enzymes* (ed. Bhatt, P.) 99–118 (Academic, 2019).
105. Ussia, M. et al. Active light-powered antibiofilm ZnO micromotors with chemically programmable properties. *Adv. Funct. Mater.* **31**, 2101178 (2021).
This article reports intrinsically asymmetric Ag-doped ZnO microrobots that photocatalytically eliminate antibiotic-resistant bacterial biofilms.
106. Li, J. et al. Water-driven micromotors for rapid photocatalytic degradation of biological and chemical warfare agents. *ACS Nano* **8**, 11118–11125 (2014).
107. Yuan, K., Jurado-Sánchez, B. & Escarpa, A. Dual-propelled lanbiotic based Janus micromotors for selective inactivation of bacterial biofilms. *Angew. Chem. Int. Ed.* **60**, 4915–4924 (2021).
108. Dong, Y. et al. Magnetic microswarm composed of porous nanocatalysts for targeted elimination of biofilm occlusion. *ACS Nano* **15**, 5056–5067 (2021).
109. Bhuyan, T. et al. Magnetotactic T-budbots to kill-n-clean biofilms. *ACS Appl. Mater. Interfaces* **12**, 43352–43364 (2020).
110. Chamas, A. et al. Degradation rates of plastics in the environment. *ACS Sustain. Chem. Eng.* **8**, 3494–3511 (2020).
111. Mitrano, D. M., Wick, P. & Nowack, B. Placing nanoplastics in the context of global plastic pollution. *Nat. Nanotechnol.* **16**, 491–500 (2021).
112. Leslie, H. A. et al. Discovery and quantification of plastic particle pollution in human blood. *Environ. Int.* **163**, 107199 (2022).
113. Sun, M. et al. Cooperative recyclable magnetic microsubmarines for oil and microplastics removal from water. *Appl. Mater. Today* **20**, 100682 (2020).
114. Ye, H. et al. Magnetically steerable iron oxides-manganese dioxide core–shell micromotors for organic and microplastic removals. *J. Colloid Interface Sci.* **588**, 510–521 (2021).
115. Villa, K., Děkanovský, L., Plutnar, J., Kosina, J. & Pumera, M. Swarming of perovskite-like Bi_2WO_6 microrobots destroy textile fibers under visible light. *Adv. Funct. Mater.* **30**, 2007073 (2020).
116. Beladi-Mousavi, S. M., Hermanová, S., Ying, Y., Plutnar, J. & Pumera, M. A maze in plastic wastes: autonomous motile photocatalytic microrobots against microplastics. *ACS Appl. Mater. Interfaces* **13**, 25102–25110 (2021).
117. Urso, M., Ussia, M. & Pumera, M. Breaking polymer chains with self-propelled light-controlled navigable hematite microrobots. *Adv. Funct. Mater.* **31**, 2101510 (2021).
This article describes the photo-Fenton degradation of polymer chains using light-powered magnetically steerable metal–haematite Janus microrobots.
118. Peng, X. et al. Eco-friendly porous iron(III) oxide micromotors for efficient wastewater cleaning. *N. J. Chem.* **43**, 12594–12600 (2019).
119. Dong, Y. et al. Graphene-based helical micromotors constructed by 'microscale liquid rope-coil effect' with microfluidics. *ACS Nano* **14**, 16600–16613 (2020).
120. Terzopoulou, A. et al. Biotemplating of metal–organic framework nanocrystals for applications in small-scale robotics. *Adv. Funct. Mater.* **32**, 2107421 (2022).
121. Ma, W., Wang, K., Pan, S. & Wang, H. Iron-exchanged zeolite micromotors for enhanced degradation of organic pollutants. *Langmuir* **36**, 6924–6929 (2020).
122. Bayraktaroğlu, M., Jurado-Sánchez, B. & Uygun, M. Peroxidase driven micromotors for dynamic bioremediation. *J. Hazard. Mater.* **418**, 126268 (2021).
123. Oral, C. M., Ussia, M. & Pumera, M. Self-propelled activated carbon micromotors for 'on-the-fly' capture of nitroaromatic explosives. *J. Phys. Chem. C* **125**, 18040–18045 (2021).
124. Mayorga-Martinez, C. C., Vyskočil, J., Novotný, F. & Pumera, M. Light-driven Ti_3C_2 MXene micromotors: self-propelled autonomous machines for photodegradation of nitroaromatic explosives. *J. Mater. Chem. A* **9**, 14904–14910 (2021).
125. Ma, E., Wang, K., Hu, Z. & Wang, H. Dual-stimuli-responsive CuS-based micromotors for efficient photo-Fenton degradation of antibiotics. *J. Colloid Interface Sci.* **603**, 685–694 (2021).
126. Feng, K., Zhang, L., Gong, J., Qu, J. & Niu, R. Visible light triggered exfoliation of COF micro/nanomotors for efficient photocatalysis. *Green Energy Environ.* https://doi.org/10.1016/j.gee.2021.09.002 (2021).
127. Tesař, J., Ussia, M., Alduhaish, O. & Pumera, M. Autonomous self-propelled MnO_2 micromotors for hormones removal and degradation. *Appl. Mater. Today* **26**, 101312 (2022).
128. Kochergin, Y. S., Villa, K., Nemeškalová, A., Kuchař, M. & Pumera, M. Hybrid inorganic–organic visible-light-driven microrobots based on donor–acceptor organic polymer for degradation of toxic psychoactive substances. *ACS Nano* **15**, 18458–18468 (2021).
129. Soto, F. et al. Rotibot: use of rotifers as self-propelling biohybrid microcleaners. *Adv. Funct. Mater.* **29**, 1900658 (2019).
130. Dekanovsky, L. et al. Chemically programmable microrobots weaving a web from hormones. *Nat. Mach. Intell.* **2**, 711–718 (2020).
This article reports bubble-propelled magnetic microrobots that weave macroscopic webs from hormones 'on the fly', facilitating their removal.
131. Peng, X., Urso, M. & Pumera, M. Photo-Fenton degradation of nitroaromatic explosives by light-powered hematite microrobots: when higher speed is not what we go for. *Small Methods* **5**, 2100617 (2021).
132. Vilela, D., Guix, M., Parmar, J., Blanco-blanes, À. & Sánchez, S. Micromotor-in-sponge platform for multicycle large-volume degradation of organic pollutants. *Small* **18**, 2107619 (2022).

133. Yang, J. et al. Micromotor-assisted highly efficient Fenton catalysis by a laccase/Fe–BTC–$NiFe_2O_4$ nanozyme hybrid with a 3D hierarchical structure. *Environ. Sci. Nano* **7**, 2573–2583 (2020).
134. Uygun, M. et al. Dye removal by laccase-functionalized micromotors. *Appl. Mater. Today* **23**, 101045 (2021).
135. Mena-Giraldo, P. & Orozco, J. Photosensitive polymeric Janus micromotor for enzymatic activity protection and enhanced substrate degradation. *ACS Appl. Mater. Interfaces* **14**, 5897–5907 (2022).
136. Chen, L., Wang, X., Lu, W., Wu, X. & Li, J. Molecular imprinting: perspectives and applications. *Chem. Soc. Rev.* **45**, 2137–2211 (2016).
137. Li, J. et al. Bioinspired Pt-free molecularly imprinted hydrogel-based magnetic Janus micromotors for temperature-responsive recognition and adsorption of erythromycin in water. *Chem. Eng. J.* **369**, 611–620 (2019).
138. Kong, L., Ambrosi, A., Nasir, M. Z. M., Guan, J. & Pumera, M. Self-propelled 3D-printed "aircraft carrier" of light-powered smart micromachines for large-volume nitroaromatic explosives removal. *Adv. Funct. Mater.* **29**, 1903872 (2019).
139. Xu, D., Yuan, H. & Ma, X. Performance of tubular micromotors in real sewage for water treatment: towards a practical scenario. *ChemNanoMat* **7**, 439–442 (2021).
140. Fu, F. & Wang, Q. Removal of heavy metal ions from wastewaters: a review. *J. Environ. Manage.* **92**, 407–418 (2011).
141. Rehman, K., Fatima, F., Waheed, I. & Akash, M. S. H. Prevalence of exposure of heavy metals and their impact on health consequences. *J. Cell. Biochem.* **119**, 157–184 (2018).
142. Jurado-Sánchez, B. et al. Self-propelled activated carbon Janus micromotors for efficient water purification. *Small* **11**, 499–506 (2015).
143. Uygun, D. A., Jurado-Sánchez, B., Uygun, M. & Wang, J. Self-propelled chelation platforms for efficient removal of toxic metals. *Environ. Sci. Nano* **3**, 559–566 (2016).
144. Maric, T. et al. Nanorobots constructed from nanoclay: using nature to create self-propelled autonomous nanomachines. *Adv. Funct. Mater.* **28**, 1802762 (2018).
145. Maric, T. et al. Microrobots derived from variety plant pollen grains for efficient environmental clean up and as an anti-cancer drug carrier. *Adv. Funct. Mater.* **30**, 2000112 (2020).
146. Yang, W. et al. Bioinspired 3D hierarchical BSA-$NiCo_2O_4$@MnO_2/C multifunctional micromotors for simultaneous spectrophotometric determination of enzyme activity and pollutant removal. *J. Clean. Prod.* **309**, 127294 (2021).
147. Gong, D., Li, B., Celi, N., Cai, J. & Zhang, D. Efficient removal of Pb(II) from aqueous systems using spirulina-based biohybrid magnetic helical microrobots. *ACS Appl. Mater. Interfaces* **13**, 53131–53142 (2021).
148. Villa, K., Manzanares Palenzuela, C. L., Sofer, Z., Matějková, S. & Pumera, M. Metal-free visible-light photoactivated C_3N_4 bubble-propelled tubular micromotors with inherent fluorescence and on/off capabilities. *ACS Nano* **12**, 12482–12491 (2018).
149. Zhang, D. et al. One-step synthesis of PCL/Mg Janus micromotor for precious metal ion sensing, removal and recycling. *J. Mater. Sci.* **54**, 7322–7332 (2019).
150. Qiu, B. et al. Interfacially super-assembled asymmetric and H_2O_2 sensitive multilayer-sandwich magnetic mesoporous silica nanomotors for detecting and removing heavy metal ions. *Adv. Funct. Mater.* **31**, 2010694 (2021).
151. Ying, Y., Pourrahimi, A. M., Sofer, Z., Matějková, S. & Pumera, M. Radioactive uranium preconcentration via self-propelled autonomous microrobots based on metal–organic frameworks. *ACS Nano* **13**, 11477–11487 (2019).
152. Guo, Z. et al. Biocatalytic metal–organic framework nanomotors for active water decontamination. *Chem. Commun.* **56**, 14837–14840 (2020).
153. Hou, T. et al. Effective removal of inorganic and organic heavy metal pollutants with poly(amino acid)-based micromotors. *Nanoscale* **12**, 5227–5232 (2020).
154. Wang, H., Khezri, B. & Pumera, M. Catalytic DNA-functionalized self-propelled micromachines for environmental remediation. *Chem* **1**, 473–481 (2016).
155. Lee, Y. et al. Sulfur-encapsulated zeolite micromotors for the selective removal of cesium from high-salt water with accelerated cleanup times. *Chemosphere* **276**, 130190 (2021).
156. Park, C. W., Kim, T., Yang, H. M., Lee, Y. & Kim, H. J. Active and selective removal of Cs from contaminated water by self-propelled magnetic illite microspheres. *J. Hazard. Mater.* **416**, 126226 (2021).
157. Vaghasiya, J. V., Mayorga-Martinez, C. C., Matějková, S. & Pumera, M. Pick up and dispose of pollutants from water via temperature-responsive micellar copolymers on magnetite nanorobots. *Nat. Commun.* **13**, 1026 (2022).
This article presents thermoresponsive magnetic nanorobots that pick up and release heavy metals and organic pollutants by changing the water temperature.
158. Beladi-Mousavi, S. M., Khezri, B., Matějková, S., Sofer, Z. & Pumera, M. Supercapacitors in motion: autonomous microswimmers for natural-resource recovery. *Angew. Chem. Int. Ed.* **58**, 13340–13344 (2019).
159. Mishra, S., Chauhan, G., Verma, S. & Singh, U. The emergence of nanotechnology in mitigating petroleum oil spills. *Mar. Pollut. Bull.* **178**, 113609 (2022).
160. Guix, M. et al. Superhydrophobic alkanethiol-coated microsubmarines for effective removal of oil. *ACS Nano* **6**, 4445–4451 (2012).
161. Gao, W. et al. Seawater-driven magnesium based Janus micromotors for environmental remediation. *Nanoscale* **5**, 4696–4700 (2013).
162. Su, Y. et al. Bubble-propelled hierarchical porous micromotors from evolved double emulsions. *Ind. Eng. Chem. Res.* **58**, 1590–1600 (2019).
163. Wang, D. et al. One-step fabrication of dual optically/magnetically modulated walnut-like micromotor. *Langmuir* **35**, 2801–2807 (2019).
164. Ma, W. & Wang, H. Magnetically driven motile superhydrophobic sponges for efficient oil removal. *Appl. Mater. Today* **15**, 263–266 (2019).
165. Wang, L., Hortelão, A. C., Huang, X. & Sánchez, S. Lipase-powered mesoporous silica nanomotors for triglyceride degradation. *Angew. Chem. Int. Ed.* **58**, 7992–7996 (2019).
This article describes enzymatic nanorobots based on lipase-modified mesoporous silica nanoparticles that accelerate oil-spill degradation.
166. Wang, L. et al. Enzyme conformation influences the performance of lipase-powered nanomotors research articles. *Angew. Chem. Int. Ed.* **59**, 21080–21087 (2020).
167. Xing, Y., Tang, S., Du, X., Xu, T. & Zhang, X. Near-infrared light-driven yolk@shell carbon@silica nanomotors for fuel-free triglyceride degradation. *Nano Res.* **14**, 654–659 (2021).
168. Some, S. et al. Microbial pollution of water with special reference to coliform bacteria and their nexus with environment. *Energy Nexus* **1**, 100008 (2021).
169. Ciofu, O., Moser, C., Jensen, P. Ø. & Høiby, N. Tolerance and resistance of microbial biofilms. *Nat. Rev. Microbiol.* **20**, 621–635 (2022).
170. Paruch, L., Paruch, A. M., Eiken, H. G. & Sørheim, R. Faecal pollution affects abundance and diversity of aquatic microbial community in anthropo-zoogenically influenced lotic ecosystems. *Sci. Rep.* **9**, 19469 (2019).
171. Clayton, G. E., Thorn, R. M. S. & Reynolds, D. M. The efficacy of chlorine-based disinfectants against planktonic and biofilm bacteria for decentralised point-of-use drinking water. *npj Clean Water* **4**, 48 (2021).
172. Qiu, W. et al. Remediation of surface water contaminated by pathogenic microorganisms using calcium peroxide: matrix effect, micro-mechanisms and morphological–physiological changes. *Water Res.* **211**, 118074 (2022).
173. Zhang, Z. et al. Micro-/nanorobots in antimicrobial applications: recent progress, challenges, and opportunities. *Adv. Healthc. Mater.* **11**, 2101991 (2022).
174. Hwang, G. et al. Catalytic antimicrobial robots for biofilm eradication. *Sci. Robot.* **4**, aaw2388 (2019).
This article reports catalytic and magnetic robots that eradicate, degrade and prevent the regrowth of bacterial biofilm.
175. Zheng, C. et al. Spirulina-templated porous hollow carbon@magnetite core-shell microswimmers. *Appl. Mater. Today* **22**, 100962 (2021).
176. Ussia, M. et al. Light-propelled nanorobots for facial titanium implants biofilms removal. *Small* **18**, e2200708 (2022).
177. Villa, K. et al. Visible-light-driven single-component $BiVO_4$ micromotors with the autonomous ability for capturing microorganisms. *ACS Nano* **13**, 8135–8145 (2019).
178. Zhang, F. et al. ACE2 receptor-modified algae-based microrobot for removal of SARS-CoV-2 in wastewater. *J. Am. Chem. Soc.* **143**, 12194–12201 (2021).
This article describes biohybrid microrobots consisting of ACE2-receptor-modified self-motile microalgae that remove SARS-CoV-2 from water.
179. Moran, J. L. & Posner, J. D. Role of solution conductivity in reaction induced charge auto-electrophoresis. *Phys. Fluids* **26**, 042001 (2014).
180. Xiao, Z. et al. Synergistic speed enhancement of an electric-photochemical hybrid micromotor by tilt rectification. *ACS Nano* **14**, 8658–8667 (2020).
181. Oral, C. M., Ussia, M. & Pumera, M. Hybrid enzymatic/photocatalytic degradation of antibiotics via morphologically programmable light-driven ZnO microrobots. *Small* **18**, 2202600 (2022).

Acknowledgements
M.P. is supported by the Grant Agency of the Czech Republic (19-26896X).

Author contributions
The manuscript was written with contributions from all authors. M. Urso and M. Ussia contributed equally.

Competing interests
The authors declare no competing interests.

Additional information
Correspondence should be addressed to Martin Pumera.

Peer review information *Nature Reviews Bioengineering* thanks Huang Tian-Yun, Jinyao Tang and the other, anonymous, reviewer(s) for their contribution to the peer review of this work.